Theory and Ultimate Strength Design of Reinforced Concrete Chimneys

Théorie et résistance limite de cheminées en béton armé

Theorie und Grenzfestigkeit von Stahlbetonschornsteinen

H. J. BRETTLE
Associate Professor, School of Civil Engineering, University of New South Wales

1. Introduction

Reinforced concrete began to replace brickwork in chimney construction late in the 19th century. In America about 400 chimneys had been constructed before 1907 indicating rapid acceptance of concrete as a satisfactory material. In recent years use of the slip forming technique has increased to the extent that related specifications are now being included in chimney design codes. The use of high strength, heat resistant concretes placed by modern handling and compacting equipment has produced exceedingly tall stacks of up to 1200 feet high [15]. Some hollow circular concrete T.V. antennas have been erected to 1700 feet [16] using similar design procedures and construction methods. No doubt the prestressing technique will be introduced for the erection of still higher thin-walled concrete structures in the near future. LEONHARDT [16] suggests that towers of "3300 feet are attainable without great difficulty".

The most comprehensive document on the design of reinforced concrete chimneys is the ACI specification 505-54 [1] in which the elastic or permissible stress design method is fully covered. Theories for the determination of stresses due to dead, wind and earthquake loadings and a differential temperature gradient across the wall thickness are included.

In this paper, the theory for the ultimate strength analysis of hollow circular sections with allowance for a large flue hole in the wall is developed and an ultimate strength design method is proposed. The theory applies to stout sections in which the column strength is assumed unaffected by slenderness ratio L/d. The relative wall thickness to diameter ratio t/d is also assumed sufficient to prevent crinkle buckling or ovalization failure of thin-walls. Failure is assumed to occur when the materials attain their ultimate strengths.

The only known experimental evidence on the ultimate strength of thin wall circular sections are the results of seven tests carried out at the University of New South Wales during 1968 and 1969. As this previously published theory [12, 13] related to bridge piers the specimens were without flue openings and not subjected to elevated temperatures. The test series supported the proposed theory within about 10%. No experimental evidence can be found in the literature on the effect of flue openings and elevated temperature on the ultimate strength of hollow circular sections. Until this has been done the theoretical approach, with due allowance for temperature effects on the material properties must be used for the ultimate strength design of reinforced concrete chimneys.

2. Temperature Effects

2.1. Material Stress-Strain Curves

Concrete stress-strain curves for axially loaded cylinders vary non-linearly from zero to the point of maximum compressive stress f'_c at a strain e'_c. Beyond this point the stress decreases with increasing strain, the relationship depending to some extent on the stiffness of the testing machine which affects the sudden rate of straining at failure. Although the ultimate strength f'_c of different concretes can be varied between wide limits, the strain e'_c at which f'_c first occurs remains reasonably constant and a value of 0.002 is usually adopted [7]. When plain concrete specimens are eccentrically loaded in compression such that tensile stress develops over portion of the specimen area, or when reinforced concrete beams are subjected to flexure, values of strain much greater than 0.002, can be measured before collapse occurs. The "Recommendations for an International Code of Practice" [7] suggests 0.0035 as the value of extreme fibre compressive strain e_{cu} at which failure occurs in such specimens. Strain values much higher than 0.0035 have been recorded in stability tests on columns in which off-loading has permitted time for measurement of these higher strains. The actual shape of the stress-strain curve for concrete is approximated by the dashed line on Fig. 1a.

The actual stress-strain curves can be approximated by a trapezoidal shape, based on the variables f'_c, e'_c and e_{cu}. This curve, first suggested by the author in 1958 [4], increases linearly from zero to the point fixed by the values f'_c and e'_c, then remains at constant stress f'_c while the strain increases to e_{cu}, when failure occurs. To adjust this trapezoidal shape to include the effect of temperature on the material properties, the parameters k_1, k_2 and k_3 are introduced where k_1 is the ratio of concrete ultimate strength at elevated

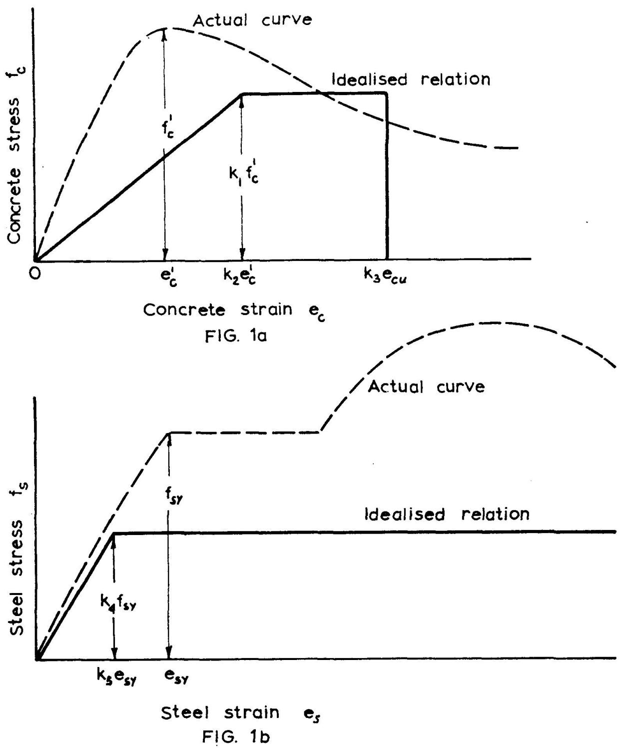

Fig. 1. Stress strain properties of concrete and steel.

temperature T to its ultimate strength at ambient temperature, k_2 is the ratio of concrete strain at elevated temperature T to its strain at ambient temperature, both strains occurring when maximum stress f_c' is first attained and k_3 is the ratio of the maximum value of extreme fibre strain in flexure at elevated temperature T to its value at ambient temperature. The idealised stress-strain curve adopted in this paper for concrete subjected to temperature rise is shown by the full line in Fig. 1 a.

The actual stress-strain curve for commercially available reinforcing steels is approximated by the dashed line in Fig. 1 b. This curve can be approximated by a stress-strain relation increasing linearly from zero to a point fixed by the yield stress f_{sy} and the yield strain e_{sy}, then remaining at constant stress f_{sy} while the strain continually increases. No upper limiting strain value has been considered. The adopted elasto-plastic shape has been adjusted for the effect of temperature by introducing parameters k_4 and k_5 where k_4 is the ratio of the steel yield stress at elevated temperature T to its yield stress f_{sy} at 20° C and k_5 is the ratio of the steel yield strain at elevated temperature T to its yield strain e_{sy} at 20° C. The adopted idealised stress-strain curve for reinforcing steels subjected to temperature is shown by the full line in Fig. 1 b.

2.2. *Effect of Temperature on Ultimate Strength*

Reinforced concrete chimneys are usually constructed with a lining of fire bricks which is separated from the concrete by an air cavity. The inner face of the concrete nevertheless reaches temperatures well above that of the outer face which is cooled by the surrounding air. A temperature gradient usually exists across the thickness of the concrete wall. This gradient depends on such factors as the thickness and diameter of the firebrick lining, the width of the air space and of the concrete wall, the coefficients of heat conductivity and transmissibility of the chimney materials, the maximum temperature and velocity of the flue gas and the surrounding air temperature. The actual inner and outer wall surface temperatures can be calculated from the equations derived in the ACI chimney code [1].

Only a few measurements of temperature variation across the wall thickness of chimneys in operation have been published. The text book on chimney design by TAYLOR and TURNER [6] reports observation of differential temperatures for five chimneys lined with firebrick and one unlined wall and in all cases the maximum concrete temperature recorded reached only 130° C. In one chimney subjected to a 530° C flue gas temperature, an 18″ firebrick lining restricted the concrete shell inner face temperature to only 70° C. These observations indicate that the concrete shell temperatures can be greatly decreased by use of linings and a ventilated air gap.

Temperature gradients across concrete shell sections of chimneys develope maximum longitudinal compressive stresses on the hot inner face and maximum longitudinal tensile stresses on the cold outer face. Using the theory given in the ACI specification [1], it can be shown that a differential temperature of 200° C across a centrally reinforced concrete wall with a steel proportion of 0.01 and a modular ratio of 12, develops maximum compressive and tensile strains on the extreme inner and outer fibres of 0.00032 and 0.00098 respectively. Assuming the simple elastic theory applies and the cross-section remains uncracked, then this compressive strain produces a compressive stress of 800 psi. Thermal stresses are usually a major portion of the total stresses produced by dead, wind and earthquake loadings under working load conditions.

At ultimate load the cross-section is usually badly cracked in flexure. Consequently the theory for computing thermal stresses no longer applies. Concrete failure occurs when the extreme fibre strain e_{cu} reaches some upper limiting value and in this paper is assumed to be 0.0035 at ambient temperature. This value increases with temperature and as indicated later has been assumed to be about 0.007 at a temperature of 600° C. As the compressive strains at ultimate loads are from about 10 to 20 times those occurring due to temperature at working loads then thermal stresses at ultimate loads will be ignored. It is however important to know the effect of elevated temperatures on the ultimate strength characteristics of the materials used in chimneys. The maximum value of the wall mean temperature has been adopted as the appropriate temperature at which to evaluate the material properties at the collapse load.

2.3. Effect of Temperature on Concrete Properties

The effect of temperature on the properties of concrete depends on the type of cement, type of aggregate, mix properties, the number of thermal cycles, the time exposed to elevated temperatures, whether the concrete is tested hot or in the cooled state, the rate of cooling or quenching in water, etc. To simplify the present discussion only Portland cement concretes will be considered. Most investigators have examined the effect of temperature on the compressive strength and modulus of elasticity of concrete but few have shown the effect on the complete stress-strain characteristics. Generally experimenters have used the ratio of the values of the material properties at elevated temperatures to their related values at ambient temperatures. The values of ambient temperatures have varied slightly at different laboratories and 20° C has been adopted as a reasonable measure of this quantity to simplify comparison of published test results.

SAEMANN and WASHA [3] measured compressive strength and modulus of elasticity and other physical characteristics of cement mortars and concretes using gravel and lightweight expanded shale aggregates when subjected to temperatures up to 230° C. The ratio k_1 for both gravel and lightweight aggregate concrete decreased about 10% at 100° C and increased about 10% at 200° C consequently this relation was approximated by a straightline of constant value $k_1 = 1.0$. The secant modulus of elasticity at 1/3 ultimate stress was reported as the modulus of elasticity in this reference. The ratio of moduli of elasticities at elevated and ambient temperatures, denoted by k_1/k_2 was for both concretes approximated by a straight line decreasing from $k_1 = 1.0$ at 20° C to $k_1 = 0.6$ at 230° C.

In 1960 ZOLDNERS [5] published test results of seven physical properties of Portland cement concretes made from gravel, sandstone, limestone and lightweight expanded slag aggregates when subjected to temperatures up to 800° C. The specimens were heated to their required temperatures and either slowly cooled or quenched in water, then dried before being finally tested at ambient temperature. When the four different aggregate concretes were slowly cooled and tested at room temperature, the strength ratio k_1 could be approximated by two straight lines, one having a constant value of $k_1 = 1.0$ up to 200° C and the other then linearly decreasing to 0.5 k_1 at 600° C. The ratio k_1 for the four types of aggregate concrete subjected to water quenching could be approximated by one straight line for k_1 decreasing from 1.0 at 20° C to 0.5 at 600° C. In both tests the limestone concrete was less affected by temperature than the gravel concrete. The moduli of elasticities were determined using the ultrasonic pulse velocity method. The ratio of the modulus of elasticity at elevated to that at ambient temperature k_1/k_2 for the slowly cooled specimens could be approximated by two straight lines, one remaining constant at $k_1/k_2 = 1.0$ up to 200° C and the other then decreasing linearly to 0.2 k_1/k_2

at 600° C. The concrete properties in a chimney heated by flue gases on the inside and subjected to downpours of rain on the outside would probably be somewhere between these two sets of experimental values. The lower conservative relation for k_1 will be considered in the present comparison.

The experimental work by HARMATHY and BERNDT [8] on hydrated Portland cement specimens and on expanded shale lightweight aggregate concrete specimens was the only reference located relating to the effect of temperature on the complete stress-strain curve of concrete or concrete materials. The effect of temperature up to 800° C on the ultimate strength f_c', modulus of elasticity E_c and the strain at failure of cylinders tested in their heated state was examined. As the load-deformation curve was obtained from the recorder of the test machine, the deformation or movement between the test machine plattens would include slackness in the test arrangement so the strain measurement would be slightly inaccurate. The tangent to the force-deformation curve at about one half of the ultimate force was used to calculate the modulus of elasticity. The values of both f_c' and E_c remained constant up to 200° C and then decreased linearly with temperature to about 70% and 50% of their respective values at 600° C. The test machine recorder obtained readings of the falling portion of the stress-strain curve slightly beyond the ultimate stress f_c' and its related strain value e_c'. However the reported maximum observed strains have been assumed equivalent to e_c' in this paper.

The contribution by CAMPBELL-ALLEN and DESAI [9] in 1967 shows a marked decrease in both compressive strength f_c' and modulus of elasticity of concrete when subjected to thermal cycles with the maximum temperature as low as 65° C. Expanded shale, fireclay brick and limestone aggregates were mixed with ordinary Portland cement using a water cement ratio of 0.4. After 20 cycles at 65° C both f_c' and E_c decreased to about 70% of their values at 20° C. After 20 cycles at 300° C, f_c' and E_c decreased to about 50% and 25% of their respective values at 20° C. This data included on Fig. 2 showed that the greatest reduction in the values of both f_c' and E_c was caused by the application of thermal cycles.

HANNANT [11] in 1967 examined the effect of continuous exposure of concrete to temperatures of about 93° C for periods of up to 18 months. Both gravel and limestone aggregates mixed with ordinary Portland cement at a water cement ratio of about 0.46 were examined. The limestone concrete strength decreased rapidly for the first three days and was 38% below its unheated control cylinder strength after being held at the steady temperature of 93° C for $1\,^1/_2$ years.

The eight authors mentioned above investigated the temperature variables most likely to deteriorate the structural properties of ordinary Portland cement concretes. In all cases their lowest observed relationships have been simplified by straight dashed line approximations in the preparation of Fig. 2. Again simple linear approximations for the lower boundaries of the stress

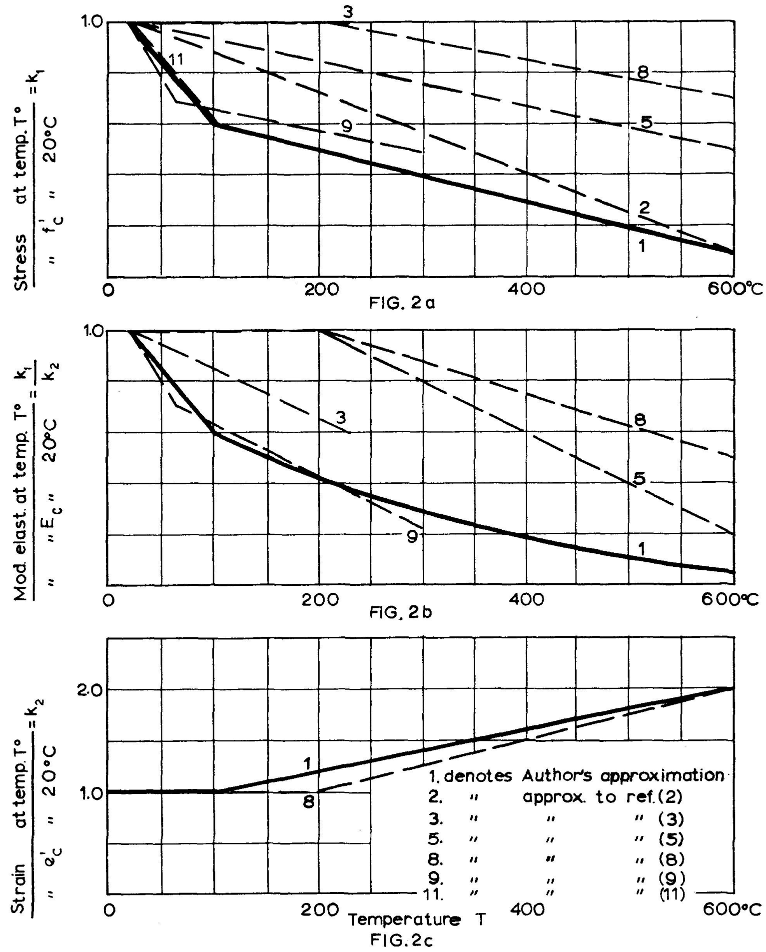

Fig. 2. Effect of temperature on concrete stress-strain properties.

parameter k_1 and the strain parameter k_2 were adopted as shown by the firm lines on Figs. 2a and 2c. The modulus of elasticity parameter k_1/k_2 was then computed and plotted as the firm line on Fig. 2b. It can be seen from Figs. 2a, 2b and 2c that the author's simplified approximations are a reasonable lower bound fit to the observed test results.

It should be noted that most of the previous authors have suggested particular cements, aggregates, water cement and aggregate cement ratios, etc., to produce better temperature resistant concretes. However it was thought prudent to adopt the lowest bound to all the observed results to obtain the most conservative estimates of the parameters k_1, k_2 and k_1/k_2 for use with the proposed theory.

No reference could be found where experimental results relate e_{cu} and temperature consequently k_3 is indefinite. It is probable that the experimental difficulties involved in measuring e_{cu} at an extreme fibre in an eccentric loading test on a column, or in a flexure test of a beam at elevated temperatures have not as yet been overcome. Until such experimental evidence becomes available the relationship between the ultimate strain e_{cu} and temperature T measured by the parameter k_3 has been assumed similar to that between the strain e_c' and T measured by the parameter k_2 i. e., $k_3 = k_2$.

It will be seen from the author's approximations in Fig. 2a that the relation between k_1 and T can be reasonably represented by two straightllines expressed by the equations,

$$\begin{aligned} 20°\,C \leqq T \leqq 100°\,C, \qquad & k_1 = -0.005\,T + 1.1, \\ 100°\,C \leqq T \leqq 600°\,C, \qquad & k_1 = -0.001\,T + 0.7. \end{aligned} \tag{1}$$

Again from the author's approximation in Fig. 2c using two straight lines, the relation between k_2 and temperature can be expressed by the equations,

$$\begin{aligned} 20°\,C \leqq T \leqq 100°\,C, \qquad & k_2 = 1.0, \\ 100°\,C \leqq T \leqq 600°\,C, \qquad & k_2 = 0.002\,T + 0.8. \end{aligned} \tag{2}$$

Using the above two approximations, the modulus of elasticity ratio k_1/k_2 at ultimate load can be calculated from Eqs. (1) and (2) and expressed by the equations,

$$\begin{aligned} 20°\,C \leqq T \leqq 100°\,C, \qquad & \frac{k_1}{k_2} = -0.005\,T + 1.1, \\ 100°\,C \leqq T \leqq 600°\,C, \qquad & \frac{k_1}{k_2} = -0.5 + \frac{1100}{2\,T + 800}. \end{aligned} \tag{3}$$

Eqs. (3) were used to compute the modulus of elasticity ratio values at particular temperatures to enable plotting the author's adopted lower bound curve shown by the firm line on Fig. 2b. It should be noted that Eqs. (3) are only included for completeness and are not used for calculation purposes in this paper.

2.4. Effect of Temperature on Steel Properties

The temperature of chimney reinforcement depends on the wall temperature gradient and on the steel position within the wall. Usually layers of steel are placed adjacent the inner and outer wall surfaces, hence the mean wall temperature is considered a reasonable measure of mean steel temperature. The maximum value of the mean wall temperature used to evaluate the concrete properties is also used to determine the steel properties at the chimney ultimate strength. The present method of design of reinforced concrete chimneys suggested by the ACI standard code 505-54 [1] is based on permissible stresses of the materials. This code suggests that the reinforcing steel used in chimneys should conform to ASTM specification for deformed bars of intermediate and hard grade steels with yield stresses of 40, and 50 ksi respectively. Consequently only hot rolled steel having a yield stress within this range will be considered to simplify the presentation in this paper.

A paper by COPELAND and WOODMAN [10] shows the experimental relation between steel yield stress f_{sy} and modulus of elasticity E_s with temperature

T up to 600° C for both hot rolled bars having yield stresses varying from 42 to 53 ksi and for cold worked steels with yield stresses from 63 to 78 ksi. The experimental curves relating f_{sy} and E_s to T for both hot rolled and cold worked steels can be approximated by two straight lines, one up to 200° C and the other within the temperature range 200° C to 600° C.

The suggested relation between k_4 and temperature T for hot rolled steel shown by the two straight lines in Fig. 3a can be found from the equations;

$$\begin{aligned} &20^\circ\,\mathrm{C} \leqq T \leqq 200^\circ\,\mathrm{C}, && k_4 = -0.00055\,T + 1.011, \\ &200^\circ\,\mathrm{C} \leqq T \leqq 600^\circ\,\mathrm{C}, && k_4 = -0.00175\,T + 1.25. \end{aligned} \tag{4}$$

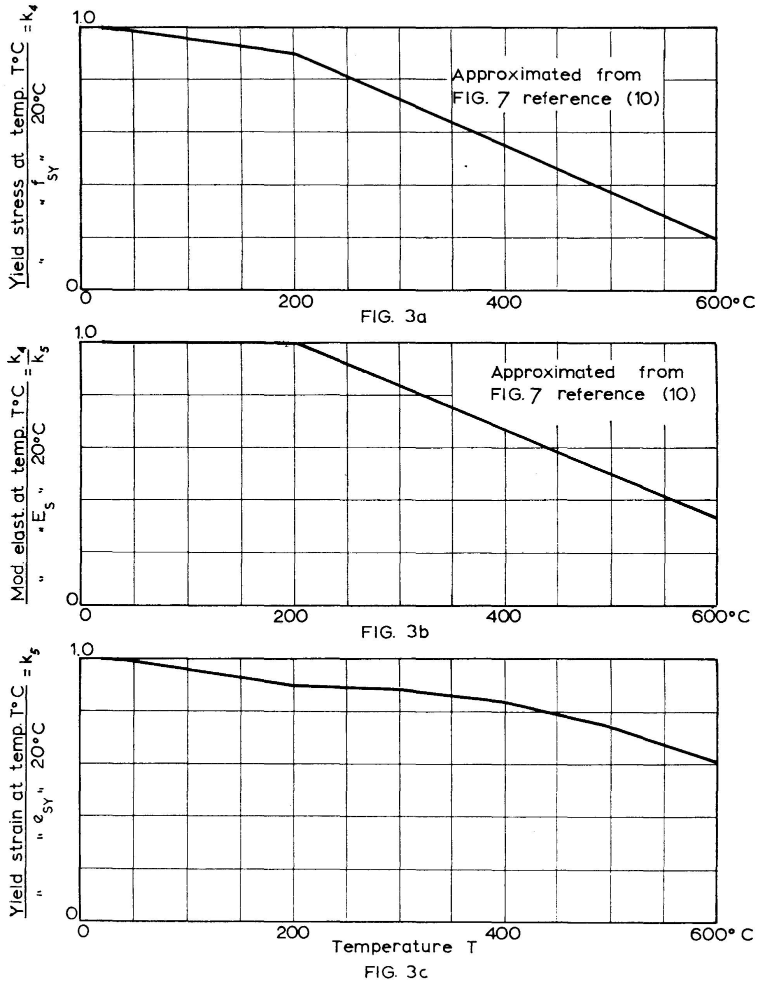

Fig. 3. Effect of temperature on steel stress-strain properties.

The relation between the ratio k_4/k_5 and temperature T can also be approximated by two straight lines as shown in Fig. 3b from which Eqs. (5) can be found.

$$\begin{aligned} &20^\circ\,\mathrm{C} \leqq T \leqq 200^\circ\,\mathrm{C}, && \frac{k_4}{k_5} = 1.0, \\ &200^\circ\,\mathrm{C} \leqq T \leqq 600^\circ\,\mathrm{C}, && \frac{k_4}{k_5} = -0.00167\,T + 1.333. \end{aligned} \tag{5}$$

From the above two sets of relations the ratio k_5 can be evaluated from Eqs. (6),

$$\begin{aligned} 20^\circ\,\mathrm{C} \leqq T \leqq 200^\circ\,\mathrm{C}, \qquad & k_5 = -0.00055\,T + 1.011, \\ 200^\circ\,\mathrm{C} \leqq T \leqq 600^\circ\,\mathrm{C}, \qquad & k_5 = 1.05 + \frac{150}{1.67\,T - 1.333}. \end{aligned} \tag{6}$$

Once the wall mean temperature is known then the parameters k_1, k_2, k_4 and k_5 can be evaluated from Eqs. (1), (2), (4) and (6).

3. Ultimate Strength Equations

The proposed ultimate strength analysis considers circular reinforced concrete sections with and without large flue openings. Wind acting from a direction opposite to the flue hole causes the greatest distress in a chimney cross-section. For a particular bending moment, the greatest concrete compressive strain e_1 develops at the flue edge indicated by point 1 in Fig. 4 and the greatest steel tensile strain e_2 occurs at point 2 in Fig. 4b. The neutral

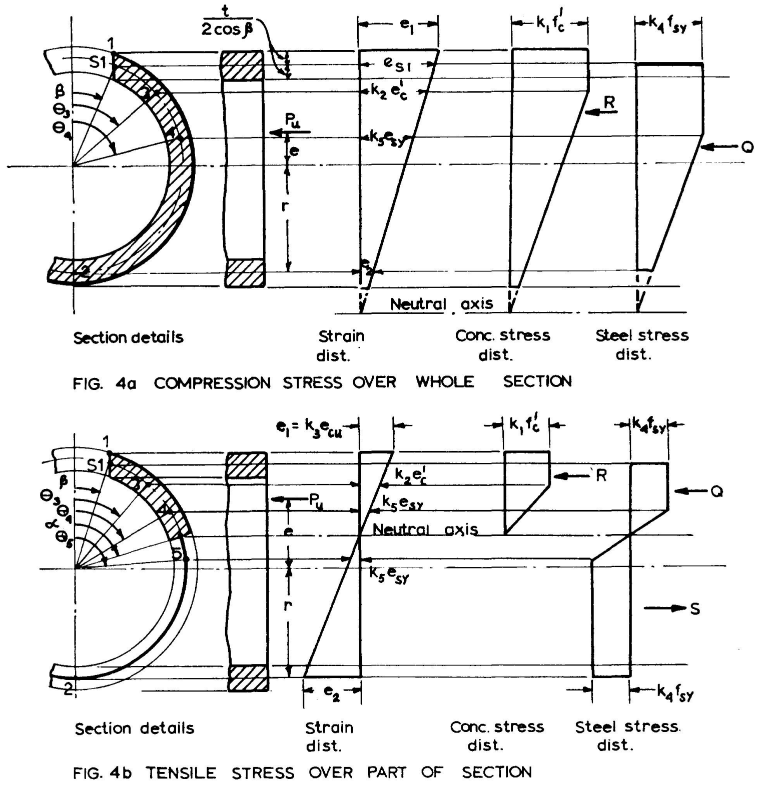

Fig. 4. Stress and strain distributions at ultimate load.

axis position is located on the chimney side away from the flue hole and its position is fixed by the e_2/e_1 ratio. The direction of the neutral axis is perpendicular to the line joining the centre of the flue hole with the centre of the circle forming the chimney section. Failure therefore occurs due to direct compression associated with uniaxial bending about this neutral axis position.

The centre of the circle forming the shape of the walls is taken as the point from which the load eccentricity is measured even though a large flue opening causes considerable shift of the true centre of gravity at this cross-section from the chimney centre line. The wall thickness has been assumed small when compared with the radius r of the section to ensure that as the section neutral axis approaches the extreme compression fibre, the integral $\int_{\beta}^{\alpha} r\,t\,d\theta$ gives a reasonable estimation of the total compression region. To assist the analysis, the individual reinforcing bars have been assumed to be replaced by a thin continuous steel shell of the same total steel area A_s and placed at the mid-wall position of the cross-section. The usual simplifying assumptions applicable to reinforced concrete structures of linear strain distribution, perfect bond between concrete and steel up to failure and the inability of concrete to sustain tensile stress have been adopted.

As described earlier the stress-strain curves for the concrete and steel are approximated by the idealised elasto-plastic curves shown by the firm lines in Fig. 1. The mean temperature T of the wall is assumed to affect the ultimate strength properties of the concrete and steel as given by the curves shown as firm lines on Figs. 2 and 3. As the analysis relates to the ultimate strength of thin wall cross-sections the effects of concrete shrinkage, creep and differential temperature stresses have been neglected.

3.1. Strain Distribution at Failure

Failure of a section is assumed to be imminent when the concrete extreme fibre strain e_1 attains some upper limiting value. When a concrete section is axially loaded such that the strain distribution is uniform all over a section then failure occurs when $e_1 = k_2 e_c'$. In the case where tensile stress exists over portion of a section i. e., when the neutral axis lies within the section as shown in Fig. 4b then failure occurs when $e_1 = k_3 e_{cu}$. For any other position of the neutral axis outside a section as shown in Fig. 4a, the extreme fibre strain e_1 attains a maximum value somewhere between these two limits. By adopting the simple relation between e_1 and the ratio e_2/e_1 as shown by two straight lines on Fig. 5, the upper limiting value of e_1 can be evaluated from either Eq. (7a) or (7b).

$$\text{For } \frac{e_2}{e_1} < 0, \qquad e_1 = k_3 e_{cu} \tag{7a}$$

$$\text{and } 0 < \frac{e_2}{e_1} < 1.0, \qquad e_1 = k_3 e_{cu} - (k_3 e_{cu} - k_2 e_c')\frac{e_2}{e_1}. \tag{7b}$$

3.11. Tension on Part of Cross-Section

The neutral axis position is located by the ratio e_2/e_1. Assuming tensile strains are positive and compressive strains are negative then the ratio e_2/e_1

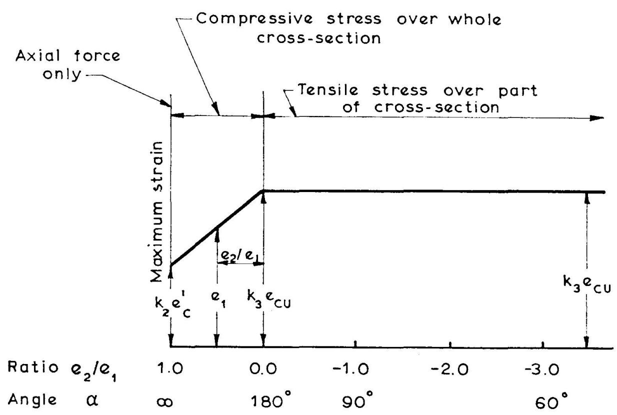

Fig. 5. Limiting values of maximum compressive strain at ultimate load.

is negative when the neutral axis is within a section. The neutral axis position can also be defined by the angle α as shown on Fig. 4b, and obtained from Eq. (8). To obviate the necessity of introducing negative signs for the e_2/e_1 ratio, its absolute value $|e_2/e_1|$ will be used when tension exists over part of the cross-section.

$$\text{For } \frac{e_2}{e_1} \leqq 0, \qquad \cos\alpha = \frac{\left|\frac{e_2}{e_1}\right|\left(\cos\beta + \frac{t}{2\,r\cos\beta}\right) + 1}{\left|\frac{e_2}{e_1}\right| - 1}. \tag{8}$$

Similarly the values of the steel extreme lower and upper fibre strains e_2 and e_{s1} respectively can be determined from Eqs. (9) and (10),

$$e_2 = \frac{k_3\,e_{cu}\,(1+\cos\alpha)}{\cos\beta - \cos\alpha + \frac{t}{2\,r\cos\beta}}, \tag{9}$$

$$e_{s1} = \frac{k_3\,e_{cu}\cos\beta}{\cos\beta - \cos\alpha + \frac{t}{2\,r\cos\beta}}. \tag{10}$$

The positions on the mean circumference where the compression strains attain the particular values $k_2\,e_c'$ and $k_5\,e_{sy}$ fixed by the angles θ_3 and θ_4 respectively are shown on Fig. 4b. These angles can be found from Eqs. (11) and (12).

$$\cos\theta_3 = \frac{k_2\,e_c'}{k_3\,e_{cu}}\left(\cos\beta - \cos\alpha + \frac{t}{2\,r\cos\beta}\right) + \cos\alpha, \tag{11}$$

$$\cos\theta_4 = \frac{k_5\,e_{sy}}{k_3\,e_{cu}}\left(\cos\beta - \cos\alpha + \frac{t}{2\,r\cos\beta}\right) + \cos\alpha. \tag{12}$$

The point on the mean circumference where the steel tensile strain equals $k_5\,e_{sy}$ is defined by the angle θ_5. From the strain distribution on Fig. 4b Eq. (13) can be found,

$$\cos\theta_5 = \cos\alpha - \frac{k_5\,e_{sy}}{k_3\,e_{cu}}\left(\cos\beta - \cos\alpha + \frac{t}{2\,r\cos\beta}\right). \tag{13}$$

The angles θ_3, θ_4 and θ_5 shown on Fig. 4b vary with the relative magnitudes of $k_2 e_c'$, $k_5 e_{sy}$, e_1, e_2 and e_{s1}.

If $e_1 \leqq k_2 e_c'$ the concrete stress distribution varies linearly and $\cos\theta_3 = \cos\theta + \frac{t}{2r\cos\beta}$. In this paper since $e_1 = k_3 e_{cu} > k_2 e_c'$, linear concrete stress distribution need not be considered.

For $e_1 \geqq k_2 e_c'$ the angle θ_3 is found from Eq. (11).

For $e_{s1} \leqq k_5 e_{sy}$ the steel does not yield in compression and $\theta_4 = \beta$.

For $e_{s1} \geqq k_5 e_{sy}$ the steel yields in compression and the angle θ_4 is found from Eq. (12).

For $e_2 \leqq k_5 e_{sy}$ the steel does not yield in tension and $\theta_5 = \pi$.

For $e_2 \geqq k_5 e_{sy}$ the steel yields in tension and the angle θ_5 is found from Eq. (13).

3.12. Compression Over Whole Cross-Section

When compressive stresses exist over the whole cross-section both extreme fibre strains are negative hence the ratio e_2/e_1 is positive. The upper limiting value of e_1 as shown by the relationship on Fig. 5 can be found from Eq. (7b). This equation can be rewritten as Eq. (14) from which the lower steel fibre strain e_2 can be evaluated. From the geometry of the strain distribution shown in Fig. 4a the strain at the upper steel fibre position e_{s1} and the angles θ_3 and θ_4 can be calculated from Eqs. (15), (16) and (17),

i.e. for $0 \leqq \frac{e_2}{e_1} \leqq 1.0$.

$$e_2 = \frac{k_3 e_{cu} e_1 - e_1^2}{k_3 e_{cu} - k_2 e_c'}, \tag{14}$$

$$e_{s1} = e_1 + \frac{(e_2 - e_1)\frac{t}{2r\cos\beta}}{1 + \cos\theta + \frac{t}{2r\cos\beta}}, \tag{15}$$

$$\cos\theta_3 = \frac{\frac{k_2 e_c'}{e_2} - \frac{e_2}{e_1}}{1 - \frac{e_2}{e_1}}\left(1 + \cos\theta + \frac{t}{2r\cos\beta}\right) - 1, \tag{16}$$

$$\cos\theta_4 = \frac{\frac{k_5 e_{sy}}{e_1} - \frac{e_2}{e_1}}{1 - \frac{e_2}{e_1}}\left(1 + \cos\theta + \frac{t}{2r\cos\beta}\right) - 1. \tag{17}$$

Depending on the relative magnitudes of $k_2 e_c'$, $k_5 e_{sy}$, e_1, e_2 and e_{s1} so the angles θ_3 and θ_4 shown on Fig. 4a vary.

If $e_1 \leqq k_2 e_c'$ the concrete stress distribution varies linearly at failure and $\cos\theta_3 = \cos\beta + \frac{t}{2r\cos\beta}$. In this paper since $e_1 \geqq k_2 e_c'$ linear concrete stress distribution need not be considered.

For $e_2 \geqq k_2 e'_c$ the concrete stress distribution remains uniform at failure and $\theta_3 = \pi$.

For $e_1 \geqq k_2 e'_c \geqq e_2$, θ_3 is found from Eq. (16).

For $e_{s1} \leqq k_5 e_{sy}$, the steel does not yield in compression and $\theta_4 = \beta$.

For $e_2 > k_2 e'_c$, the steel stress remains uniform and $\theta_4 = \pi$.

For $e_{s1} > k_5 e_{sy} > e_2$, θ_4 is found from Eq. (17).

3.2. Equilibrium Conditions

3.21. Tension on Part of Cross-Section

The steel and the concrete stress distributions for the case where the neutral axis is inside the section at failure is shown on Fig. 4b. With the wall thickness t assumed small in comparison with the mean radius r, the concrete stress may be expressed as a function of the variable angle θ.

$$\text{For } \beta < \theta < \theta_3, \qquad f_c = k_1 f'_c.$$

$$\text{For } \theta_3 < \theta < \alpha, \qquad f_c = \frac{k_1 f'_c (\cos\theta - \cos\alpha)}{\cos\theta_3 - \cos\alpha}.$$

A small concrete elemental area in compression subtended by an angle $d\theta$ at the geometric centre is $(1-p)\, r\, t\, d\theta$. The compressive force acting on this concrete element is $dR = f_c (1-p)\, r\, t\, d\theta$.

The total compressive force in the concrete above the neutral axis is then,

$$R = 2\int_{\theta=\beta}^{\theta_3} k_1 f'_c (1-p)\, r\, t\, d\theta + 2\int_{\theta=\theta_3}^{\alpha} \frac{k_1 f'_c (\cos\theta - \cos\alpha)(1-p)\, r\, t\, d\theta}{\cos\theta_3 - \cos\alpha},$$

i.e.

$$R = 2 k_1 f'_c (1-p)\, r\, t\, A_1, \tag{18}$$

where

$$A_1 = \theta_3 - \beta + \frac{\sin\alpha - \sin\theta_3 + (\theta_3 - \alpha)\cos\alpha}{\cos\theta_3 - \cos\alpha}.$$

For thin wall sections e_{s1} approaches e_1 and for this case $e_1 = k_3 e_{cu}$. The ACI chimney code [1] does not permit $k_4 f_{sy} > 60$ ksi. Since in this paper $e_{s1} > k_4 e_{sy}$ a discontinuity will always occur in the idealized steel stress distribution at failure as indicated on Fig. 4b and no other steel compressive stress distribution need be considered.

The compressive steel stresses are,

$$\text{for } \beta \leqq \theta \leqq \theta_4, \qquad f_s = k_4 f_{sy},$$

$$\text{for } \theta_4 \leqq \theta \leqq \alpha, \qquad f_s = \frac{k_4 f_{sy} (\cos\theta - \cos\alpha)}{\cos\theta_4 - \cos\alpha}$$

and the total compressive force in the steel becomes,

$$Q = 2\int_{\theta=\beta}^{\theta_4} k_4 f_{sy}\, p\, r\, t\, d\theta + 2\int_{\theta=\theta_4}^{\alpha} \frac{k_4 f_{sy}(\cos\theta - \cos\alpha)\, p\, r\, t\, d\theta}{\cos\theta_4 - \cos\alpha},$$

i.e.
$$Q = 2 k_4 f_{sy}\, p\, r\, t\left[\theta_4 - \beta + \frac{\sin\alpha - \sin\theta_4 + (\theta_4 - \alpha)\cos\alpha}{\cos\theta_4 - \cos\alpha}\right]. \tag{19}$$

For small eccentricities of loading it is possible for $e_2 \leqq k_5 e_{sy}$ and in this case the steel will not yield in tension.

$$\text{For } \alpha \leqq \theta \leqq \pi, \qquad f_s = \frac{k_4 f_{sy} e_2 (\cos\alpha - \cos\theta)}{k_5 e_{sy}(1+\cos\alpha)}$$

and the total tensile force in the steel is

$$S = 2\int_{\theta=\alpha}^{\pi} \frac{k_4 f_{sy} e_2\, p\, r\, t(\cos\alpha - \cos\theta)\, d\theta}{k_5 e_{sy}(1+\cos\alpha)} = \frac{2 k_4 f_{sy} e_2\, p\, r\, t[\sin\alpha + (\pi-\alpha)\cos\alpha]}{k_5 e_{sy}(1+\cos\alpha)}. \tag{20}$$

For larger eccentricities of loading i.e., when $e_2 > k_5 e_{sy}$ a discontinuity will occur in the idealized steel stress distribution at failure as indicated on Fig. 4b.

The tensile steel stress then becomes,

$$\text{for } \alpha \leqq \theta \leqq \theta_5, \qquad f_s = \frac{k_4 f_{sy}(\cos\alpha - \cos\theta)}{\cos\alpha - \cos\theta_5},$$

$$\text{for } \theta_5 \leqq \theta \leqq \pi, \qquad f_s = k_4 f_{sy}$$

and the total tensile force in the steel is,

$$S = 2\int_{\theta=\alpha}^{\theta_5} \frac{k_4 f_{sy}\, p\, r\, t(\cos\alpha - \cos\theta)}{\cos\alpha - \cos\theta_5} d\theta + 2\int_{\theta=\theta_5}^{\pi} k_4 f_{sy}\, p\, r\, t\, d\theta,$$

i.e.
$$S = 2 k_4 f_{sy}\, p\, r\, t\left[\pi - \theta_5 + \frac{\sin\alpha - \sin\theta_5 + (\theta_5 - \alpha)\cos\alpha}{\cos\alpha - \cos\theta_5}\right]. \tag{20a}$$

Equilibrium of forces requires that,

$$P_u = R + Q - S.$$

This equation can be expressed in non-dimensionalised form as,

$$\frac{P_u}{2 k_1 f_c'(1-p)\, r\, t} = A_1 + q B_1, \tag{21}$$

where
$$q = \frac{k_4 f_{sy}\, p}{k_1 f_c'(1-p)},$$

where for $e_2 \leqq k_5 e_{sy}$,

$$B_1 = \theta_4 - \beta + \frac{\sin\alpha - \sin\theta_4 + (\theta_4 - \alpha)\cos\alpha}{\cos\theta_4 - \cos\alpha} + \frac{\left|\frac{e_2}{e_1}\right|[\sin\alpha + (\pi-\alpha)\cos\alpha]}{\frac{k_5 e_{sy}}{e_1}(1+\cos\alpha)},$$

for $e_2 \geqq k_5 e_{sy}$,

$$B_1 = \theta_4 + \theta_5 - \beta - \pi + \frac{\sin\alpha - \sin\theta_4 + (\theta_4 - \alpha)\cos\alpha}{\cos\theta_4 - \cos\alpha} - \frac{\sin\alpha - \sin\theta_5 + (\theta_5 - \alpha)\cos\alpha}{\cos\alpha - \cos\theta_5}.$$

A second equilibrium equation is obtained by considering the moments of forces about the neutral axis of the section. This yields the following equation,

$$P_u(e - r\cos\alpha) = R' + Q' + S',$$

where R', Q' and S' are respectively, the moments of the forces R, Q, and S about this axis. The moment of the force applied to a small concrete elemental area $(1-p)\,r\,t\,d\theta$ acting at a distance $r\ (\cos\theta - \cos\alpha)$ from the neutral axis is,

$$dR' = f_c(1-p)\,r^2 t(\cos\theta - \cos\alpha)\,d\theta$$

and

$$R' = 2\int_{\theta=\beta}^{\theta_3} k_1 f_c'(1-p)\,r^2 t(\cos\theta - \cos\alpha)\,d\theta + 2\int_{\theta=\theta_3}^{\alpha} \frac{k_1 f_c'(1-p)\,r^2 t(\cos\theta - \cos\alpha)^2\,d\theta}{\cos\theta_3 - \cos\alpha},$$

i.e.

$$R' = 2k_1 f_c'(1-p)\,r^2 t\,C_1, \tag{22}$$

where $C_1 = \sin\theta_3 - \sin\beta + (\beta - \theta_3)\cos\alpha$

$$+\frac{(\alpha - \theta_3)(0.5 + \cos^2\alpha) - 1.5\sin\alpha\cos\alpha - 0.5\sin\theta_3\cos\theta_3 + 2\cos\alpha\sin\theta_3}{\cos\theta_3 - \cos\alpha}.$$

The moment Q' is obtained from the integral,

$$Q' = 2\int_{\theta=\beta}^{\theta_4} k_4 f_{sy}\,p\,r^2 t(\cos\theta - \cos\alpha)\,d\theta + 2\int_{\theta=\theta_4}^{\alpha} \frac{k_4 f_{sy}\,p\,r^2 t(\cos\theta - \cos\alpha)^2\,d\theta}{\cos\theta_4 - \cos\alpha},$$

i.e.

$$Q' = 2k_4 f_{sy}\,p\,r^2 t\Big[\sin\theta_4 - \sin\beta + (\beta - \theta_4)\cos\alpha$$

$$+\frac{(\alpha - \theta_4)(0.5 + \cos^2\alpha) - 1.5\sin\alpha\cos\alpha - 0.5\sin\theta_4\cos\theta_4 + 2\cos\alpha\sin\theta_4}{\cos\theta_4 - \cos\alpha}\Big]. \tag{23}$$

For small eccentricities i.e. when $e_2 \leqq k_5 e_{sy}$ the steel will not yield in tension. For $\alpha \leqq \theta \leqq \pi$ the total moment S' of the steel tensile force about the neutral axis becomes,

$$S' = 2\int_{\theta=\alpha}^{\pi} \frac{k_4 f_{sy} e_2\,p\,r^2 t(\cos\alpha - \cos\theta)^2\,d\theta}{k_5 e_{sy}(1+\cos\alpha)} = \frac{2k_4 f_{sy} e_2\,p\,r^2 t[(\pi - \alpha)(0.5 + \cos^2\alpha) + 1.5\sin\alpha\cos\alpha]}{k_5 e_{sy}(1+\cos\alpha)}. \tag{24}$$

For $e_2 \geqq k_5 e_{sy}$ the moment S' is likewise given by the integral,

$$S' = 2\int_{\theta=\alpha}^{\theta_5} \frac{k_4 f_{sy}\,p\,r^2 t(\cos\alpha - \cos\theta)^2\,d\theta}{\cos\alpha - \cos\theta_5} + 2\int_{\theta=\theta_5}^{\pi} k_4 f_{sy}\,p\,r^2 t(\cos\alpha - \cos\theta)\,d\theta,$$

i.e. $$S' = 2\,k_4 f_{sy}\, p\, r^2 t \Bigg[\sin\theta_5 + (\pi-\theta_5)\cos\alpha + \frac{(\theta_5-\alpha)(0.5+\cos^2\alpha)+1.5\sin\alpha\cos\alpha+0.5\sin\theta_5\cos\theta_5-2\cos\alpha\sin\theta_5}{\cos\alpha-\cos\theta_5}\Bigg]. \tag{24a}$$

The moment equilibrium equation can be expressed in non-dimensional form as,

$$\frac{P_u(e-r\cos\alpha)}{2\,k_1 f_c'(1-p)\,r^2 t} = C_1 + q\,D_1, \tag{25}$$

where for $e_2 \leqq k_5\, e_{sy}$

$$D_1 = \sin\theta_4 - \sin\beta + (\beta-\theta_4)\cos\alpha + \frac{(\alpha-\theta_4)(0.5+\cos^2\alpha)-1.5\sin\alpha\cos\alpha-0.5\sin\theta_4\cos\theta_4+2\cos\alpha\sin\theta_4}{\cos\theta_4-\cos\alpha} + \frac{\left|\frac{e_2}{e_1}\right|[(\pi-\alpha)(0.5+\cos^2\alpha)+1.5\sin\alpha\cos\alpha]}{\frac{k_5\, e_{sy}}{e_1}(1+\cos\alpha)}$$

and for $e_2 \geqq k_5\, e_{sy}$

$$D_1 = \sin\theta_4 + \sin\theta_5 - \sin\beta + (\beta-\theta_4)\cos\alpha + (\pi-\theta_5)\cos\alpha + \frac{(\alpha-\theta_4)(0.5+\cos^2\alpha)-1.5\sin\alpha\cos\alpha-0.5\sin\theta_4\cos\theta_4+2\cos\alpha\sin\theta_4}{\cos\theta_4-\cos\alpha} + \frac{(\theta_5-\alpha)(0.5+\cos^2\alpha)+1.5\sin\alpha\cos\alpha+0.5\sin\theta_5\cos\theta_5-2\cos\alpha\sin\theta_5}{\cos\alpha-\cos\theta_5}.$$

It should be noted that the terms A_1, B_1, C_1 and D_1 are all non-dimensional as they are derived from trigonometric functions of the angles α, β, θ_3, θ_4, θ_5 and π and the strain ratios $\frac{e_2/e_1}{k_2\, e_c'/e_1}$ and $\frac{e_2/e_1}{k_5\, e_{sy}/e_1}$.

From Eqs. (21) and (25) the eccentricity ratio e/r becomes,

$$\frac{e}{r} = \cos\alpha + \frac{C_1+q\,D_1}{A_1+q\,B_1}. \tag{26}$$

The concrete area A_c and the steel area A_s of a chimney with a flue hole in the wall are respectively, $A_c = 2\,(1-p)\,r\,t\,(\pi-\beta)$ and $A_s = 2\,p\,r\,t\,(\pi-\beta)$.

In this paper the steel area is assumed uniformly distributed around the mid-wall position consequently the geometric and plastic centroids of both areas are located at the same position. A load placed at this position causes uniform stress and strain across a section and is defined as the axial load P_0, where $P_0 = 2\,k_1 f_c'(1-p)\,r\,t\,(\pi-\beta) + 2\,f_s\,p\,r\,t\,(\pi-\beta)$. When $k_2\, e_c' < k_5\, e_{sy}$ the steel does not yield before the concrete fails and,

$$f_s = \frac{k_4\, f_{sy}\,\frac{k_2\, e_c'}{e_1}}{\frac{k_5\, e_{sy}}{e_1}},$$

i.e.
$$P_0 = 2\,k_1 f_c'(1-p)\,r\,t\,(\pi-\beta)\left(1+\frac{\frac{k_2 e_c'}{e_1}}{\frac{k_5 e_{sy}}{e_1}}q\right). \tag{27}$$

From Eqs. (21) and (27) the chimney ultimate strength ratio P_u/P_0 becomes,

$$\frac{P_u}{P_0} = \frac{A_1+q\,B_1}{(\pi-\beta)\left(1+\frac{k_2 e_c'/e_1}{k_5 e_{sy}/e_1}q\right)}. \tag{28}$$

When $k_2 e_c' \geqq k_5 e_{sy}$ the steel yields before concrete failure and $f_s = f_{sy}$

i.e.
$$P_0 = 2\,k_1 f_c'(1-p)\,r\,t\,(\pi-\beta)\,(1+q) \tag{27a}$$

and
$$\frac{P_u}{P_0} = \frac{A_1+q\,B_1}{(\pi-\beta)\,(1+q)}. \tag{28a}$$

3.22. Compression Over Whole of Cross-Section

The stress distribution for the case where the neutral axis is outside the section at failure is shown in Fig. 4a. When t is small compared with r the concrete stress expressed as a function of θ becomes,

for $\beta \leqq \theta \leqq \theta_3$, $\quad f_c = k_1 f_c'$,

for $\theta_3 \leqq \theta \leqq \pi$, $\quad f_c = \dfrac{k_1 f_c'}{1+\cos\theta_3}\left[1+\cos\theta+\dfrac{e_2}{k_2 e_c'}(\cos\theta_3-\cos\theta)\right]$,

A small concrete radial elemental area subtended by an angle $d\theta$ at the geometric centre is $(1-p)\,r\,t\,d\theta$. The compressive force acting on this concrete element is $d\,R = f_c(1-p)\,r\,t\,d\theta$.

The total compressive force in the concrete is,

$$R = 2\int_{\theta=\beta}^{\theta_3} k_1 f_c'(1-p)\,r\,t\,d\theta + 2\int_{\theta=\theta_3}^{\pi} \frac{k_1 f_c'(1-p)\,r\,t}{1+\cos\theta_3}\left[1+\cos\theta+\frac{e_2}{k_2 e_c'}(\cos\theta_3-\cos\theta)\right]d\theta,$$

i.e.
$$R = 2\,k_1 f_c'(1-p)\,r\,t\,A_2, \tag{29}$$

where
$$A_2 = \theta_3-\beta+\frac{\pi-\theta_3-\sin\theta_3+\frac{e_2/e_1}{k_2 e_c'/e_1}[(\pi-\theta_3)\cos\theta_3+\sin\theta_3]}{1+\cos\theta_3}.$$

For $e_2 > k_2 e_c'$, $\theta_3 = \pi$ and R can again be found from Eq. (29). The steel stresses may also be expressed as a function of the variable angle θ.

For $\beta \leqq \theta \leqq \theta_4$, $\quad f_s = k_4 f_{sy}$.

For $\theta_4 \leqq \theta \leqq \pi$, $\quad f_s = \dfrac{k_4 f_{sy}}{1+\cos\theta_4}\left[1+\cos\theta+\dfrac{e_2}{k_5 e_{sy}}(\cos\theta_4-\cos\theta)\right]$

and the total compressive force in the steel becomes,

$$Q = 2 f_{sy} p r t B_2, \tag{30}$$

where $$B_2 = \theta_4 - \beta + \frac{\pi - \theta_4 - \sin\theta_4 + \frac{e_2/e_1}{k_5\, e_{sy}/e_1}[(\pi-\theta_4)\cos\theta_4 + \sin\theta_4]}{1+\cos\theta_4}.$$

For $e_{s1} < k_5 e_{sy}$, $\theta_4 = \beta$ and for $e_2 > k_2 e_c'$, $\theta_4 = \pi$. Eq. (30) can again be used to evaluated Q for these two cases provided the steel yields. Otherwise Eq. (30) is multiplied by e_{s1}/e_{sy} to convert f_{sy} to the steel stress at point $s\,1$ shown on Fig. 4.

Equilibrium of forces requires that,

$$P_u = R + Q.$$

This equation can be expressed in non-dimensional form as,

$$\frac{P_u}{2 k_1 f_c' (1-p) r t} = A_2 + q B_2. \tag{31}$$

A second equilibrium equation is obtained by equating moments of internal and external forces. It is convenient to take moments about an axis passing through the lower steel fibre where the strain is e_2.

The following equation is then obtained,

$$P_u (e + r) = R' + Q',$$

where the moments of R and Q about this axis are denoted by R' and Q' respectively. The moment of the force applied to a small concrete elemental area $(1-p) r t\, d\theta$ acting at a distance $r(1+\cos\theta)$ from the lower fibre is,

$$dR' = f_c (1-p) r^2 t (1+\cos\theta)\, d\theta$$

and $$R' = 2\int_{\theta=\beta}^{\theta_3} k_1 f_c' (1-p) r^2 t (1+\cos\theta)\, d\theta$$

$$+ 2\int_{\theta=\theta_3}^{\pi} \frac{k_1 f_c' (1-p) r^2 t}{1+\cos\theta_3}\left[1+\cos\theta + \frac{e_2}{k_2 e_c'}(\cos\theta_3 - \cos\theta)\right](1+\cos\theta)\, d\theta,$$

i.e. $$R' = 2 k_1 f_c' (1-p) r^2 t C_2, \tag{32}$$

where $$C_2 = \theta_3 - \beta + \sin\theta_3 - \sin\beta + \left[\frac{1.5(\pi-\theta_3) - 0.5\sin\theta_3\cos\theta_3 - 2\sin\theta_3}{1+\cos\theta_3}\right.$$

$$\left. + \frac{\frac{e_2/e_1}{k_2\, e_c'/e_1}[(\pi-\theta_3)(\cos\theta_3 - 0.5) + \sin\theta_3 - 0.5\sin\theta_3\cos\theta_3]}{1+\cos\theta_3}\right].$$

For $e_2 \geqq k_2 e_c'$, $\theta_3 = \pi$ and R' can again be found from Eq. (32). In a similar manner, the moment of the steel force about the lower extreme fibre may be expressed as,

$$Q' = 2\,k_4 f_{sy}\,p\,r^2\,t\,D_2, \tag{33}$$

where $$D_2 = \theta_4 - \beta + \sin\theta_4 - \sin\beta + \left[\frac{1.5\,(\pi-\theta_4) - 0.5\cos\theta_4\sin\theta_4 - 2\sin\theta_4}{1+\cos\theta_4}\right.$$
$$\left. + \frac{\frac{e_2/e_1}{k_4\,e_{sy}/e_1}\,[(\pi-\theta_4)(\cos\theta_4 - 0.5) - 0.5\sin\theta_4\cos\theta_4 + \sin\theta_4]}{1+\cos\theta_4}\right].$$

For $e_{s1} \leqq k_5\,e_{sy}$, $\theta_4 = \beta$ and for $e_2 = k_2\,e_c'$, $\theta_4 = \pi$.

Eq. (33) can again be used to evaluate Q' for these two cases, provided the steel yields otherwise Eq. (30) is multiplied by e_{s1}/e_{sy} to convert f_{sy} to the steel stress at point $s\,1$ shown on Fig. 4. Again it should be noted that the terms A_2, B_2, C_2 and D_2 are all non-dimensional as they are derived from trigonometric functions of the angles β, θ_3, θ_4 and π and the strain ratios $\frac{e_2/e_1}{k_2\,e_c'/e_1}$ and $\frac{e_2/e_1}{k_5\,e_{sy}/e_1}$.

The moment equilibrium equation can be expressed in non-dimensional form as,

$$\frac{P_u\,(e+r)}{2\,k_1 f_c'\,(1-p)\,r^2\,t} = C_2 + q\,D_2. \tag{34}$$

From Eqs. (31) and (34) the eccentricity ratio e/r becomes,

$$\frac{e}{r} = \frac{C_2 + q\,D_2}{A_2 + q\,B_2} - 1. \tag{35}$$

The axial capacity P_0 of a hollow circular section at failure is given either by Eq. (27) or (27a). From Eqs. (27) or (27a) and (31) the chimney ultimate strength ratio P_u/P_0 becomes,

$$\frac{P_u}{P_0} = \frac{A_2 + q\,B_2}{(\pi-\beta)(1+q)}. \tag{36}$$

4. Ultimate Strength Design

4.1. Design Charts

The theory has been presented in non-dimensional form to minimise the number of design charts for the large number of variables involved. The charts were produced to facilitate the direct proportioning of satisfactory chimney sections using the ultimate strength approach with minimum effort on the part of designers.

A computer programme written in Fortran IV language produced the data required for the design charts. The values of e_c', e_{cu}, e_{sy}, $t/2\,r$ and β were read into the programme for each particular case and the strain values at ambient temperature were modified when necessary for elevated temperatures up to

600° C. The ratio e_2/e_1 which located the position of the neutral axis was then varied from -15.0 to 1.0 in 0.05 increments. The upper limiting value of strain e_1 at which the concrete section was assumed to fail was fixed. Depending on the position of the neutral axis with respect to the cross-section and to the relative magnitudes of the material strains, the strain ratios $k_2 e_c'/e_1$ and $k_5 e_{sy}/e_1$ were calculated and the angles α, θ_3, θ_4, and θ_5 computed. The trigonometrical functions A_1, B_1, C_1, D_1, A_2, B_2, C_2 and D_2 were then evaluated.

To allow for material strengths $k_1 f_c'$ and $k_4 f_{sy}$ and the proportion of steel p, the steel ratio parameter q was introduced and varied from 0 to 1.0 in 0.1 increments. The ratios e/r and P_u/P_0 were then computed for the production of the ultimate strength design charts. The programme was run on an IBM 360/50 system computer for an extensive range of input data and design charts prepared for three different flue openings and four different grades of steel.

For vertical circular chimneys self weight acts along the centre of the circle forming the cross-section shape and the eccentricity e of this loading as defined in the notation is zero. For chimneys P_u is a maximum when it equals P_0 i.e., when it is located at the plastic centroid of the section. The introduction of a flue hole shifts the plastic centroid away from the centre of the circular shape. In these cases the shift of the plastic centroid is indicated by the maximum value of negative eccentricity shown on the related design charts. The effect of the self weight bending moment at a flue position has already been included in the design graphs where it can be seen that although e equals zero the P_u/P_0 ratio is less than it's maximum value. When using the included design charts only the moments of forces about the centre of the circular shape need be considered.

4.2. Effect of Ratio $t/2r$

In deriving the theory, the stress f_c was assumed uniform over a small elemental area $r t d\theta$ and $\int_{\theta=\beta}^{\alpha} r t (1-p)\, d\theta$ taken as a reasonable estimate of the total concrete area above the neutral axis. This is reasonably true provided $t/2r$ is small. When $t/2r$ is assumed to be zero point 1 becomes point $s1$ on Fig. 4 and $e_1 = e_{s1}$. This approximation simplifies the algebra and greatly reduces the required number of design charts. For the particular case shown on Fig. 6, it can be seen that as $t/2r$ changes from 0 to 0.2 the ultimate strength ratio changes by a maximum of about 2%. This minor effect does not appear to warrant the use of additional design charts and in the preparation of Figs. 9a to 12c the $t/2r$ ratio was taken as zero.

It should be noted that whereas $t/2r$ has little effect on the P_u/P_0 ratio, Eqs. (27) and (27a) show that the thickness t has a decisive effect on P_0. This is turn has a direct effect on P_u.

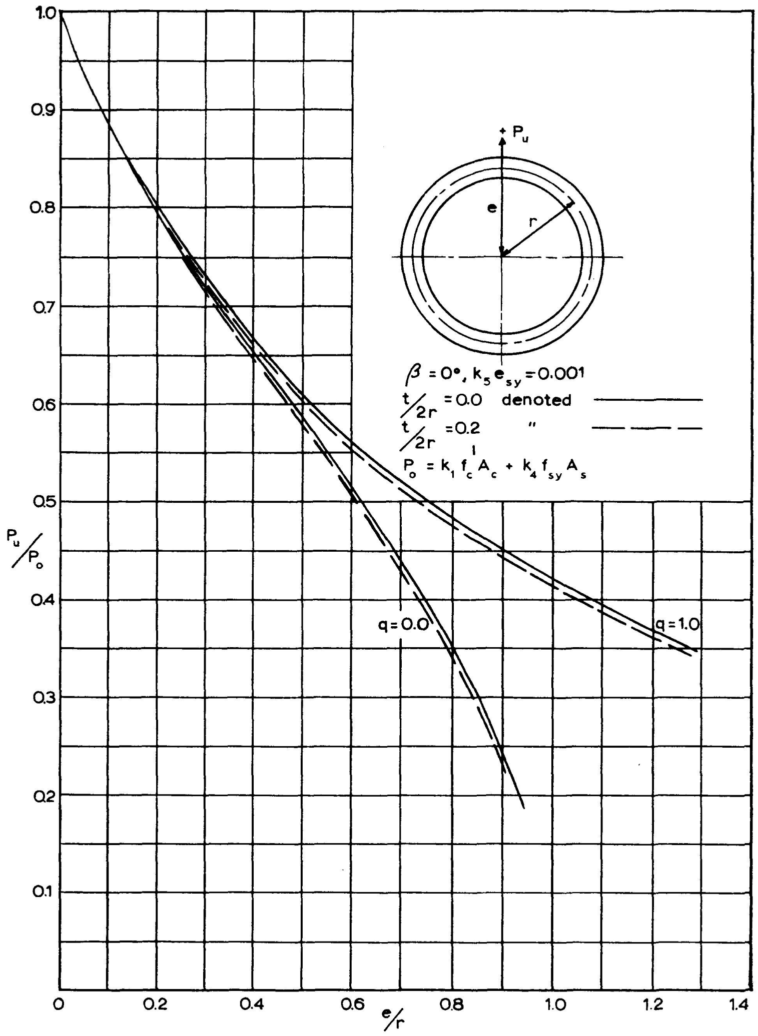

Fig. 6. Comparison of wall thickness ratio $t/2r$ variation.

4.3. Effect of Ratio $k_2 e_c'/e_1$

One set of experimental results shown on Fig. 2c indicated that the strain $k_2 e_c'$ increases 100% as the wall temperature T changes from 20° C to 600° C. No experimental results could be found for the strain $k_3 e_{cu}$ and it was assumed that $k_3 = k_2$. Only the ratio $k_2 e_c'/e_1$ is used in estimating the chimney ultimate strength. When tension acts on part of the cross-section this ratio becomes $k_2 e_c'/k_3 e_{cu}$ and when compression acts over the whole area it becomes $k_2 e_c'/(k_3 e_{cu} - \frac{e_2}{e_1}(k_3 e_{cu} - k_2 e_c'))$. Since $k_2 = k_3$ both strain ratios become independent of temperature.

The ratio $k_2 e_c'/e_1$ determines the shape of the concrete stress strain relation and hence the shape of the concrete stress block. In this paper the values adopted for e_c', and e_{cu} were 0.002 and 0.0035 respectively. Assuming a 50% increase in e_c' the particular section shown on Fig. 7a indicates a maximum variation in the ultimate strength ratio P_u/P_0 of about 3%.

Again assuming a 100% increase in e_{cu}, the particular section shown on

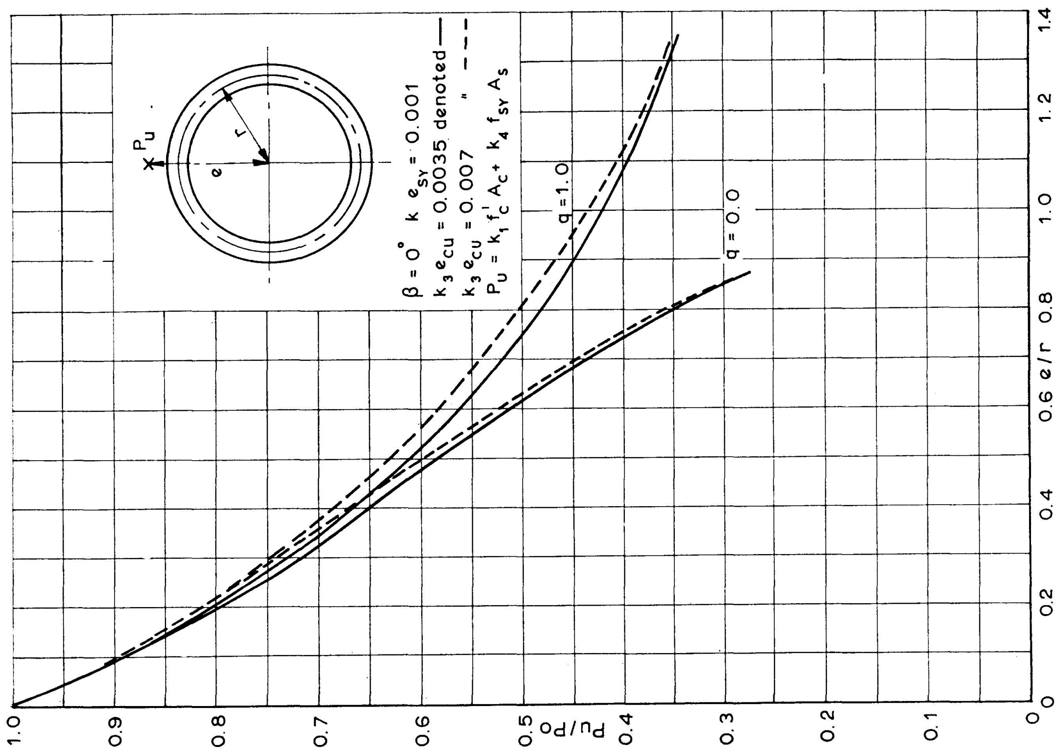

Fig. 7b. Comparison of concrete strain $k_3 e_{cu}$ variation.

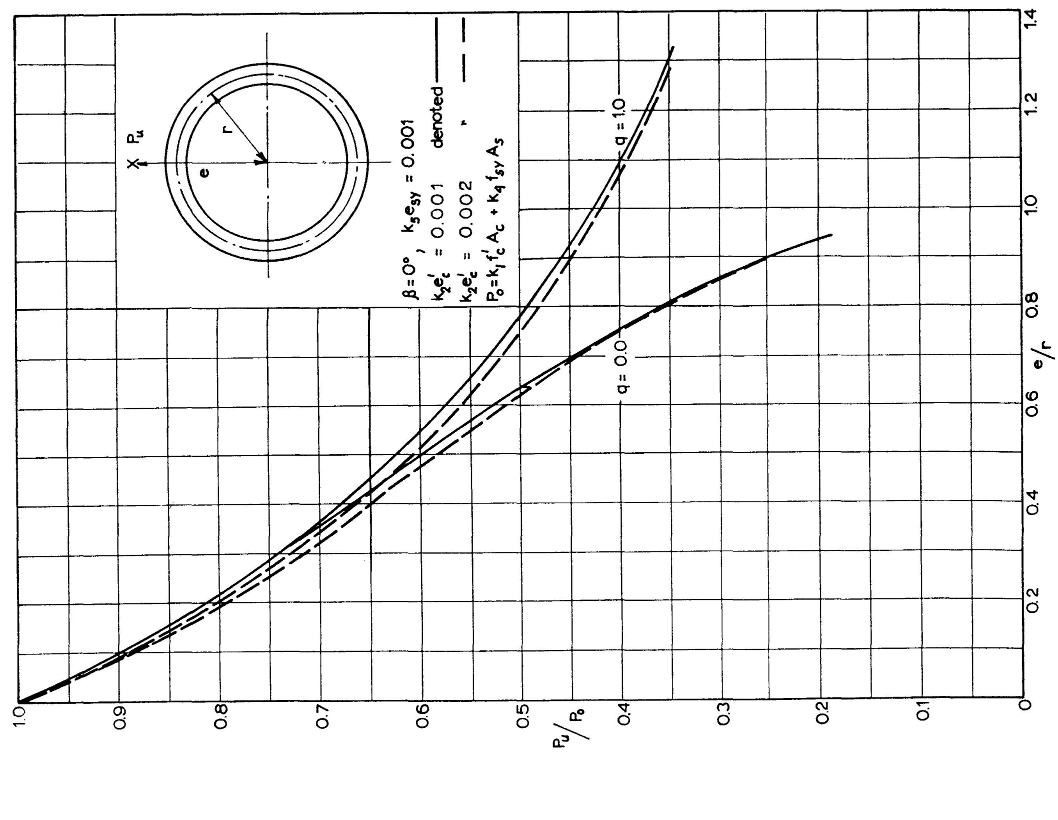

Fig. 7a. Comparison of concrete strain $k_2 e'_c$ variation.

Fig. 7b indicates a maximum variation in P_u/P_0 of about 4%. These small changes in P_u/P_0 do not warrant changing either e_c' or e_{cu} and the values of 0.002 and 0.0035 were used when computing the data for all the included design charts.

4.4. Effect of Ratio $k_5\,e_{sy}/e_1$

The steel yield strain $k_5\,e_{sy}$ shown on Fig. 3c decreases by 40% as the temperature T changes from 20° C to 600° C. Only the ratio $k_5\,e_{sy}/e_1$ is used in computing the chimney ultimate strength. When tension acts on part of the cross-section this ratio becomes $k_5\,e_{sy}/k_3\,e_{cu}$ and when compression acts over the whole area it changes to $k_5\,e_{sy}/(k_3\,e_{cu}-\frac{e_2}{e_1}(k_3\,e_{cu}-k_2\,e_c'))$ and as $k_3=k_2$ this ratio becomes $k_5\,e_{sy}/k_2\,(e_{cu}-\frac{e_2}{e_1}(e_{cu}-e_c'))$. Assuming a 100% increase in both $k_2\,e_c'$ and $k_3\,e_{cu}$, the particular section shown in Fig. 8a shows a maximum variation in P_u/P_0 of about 3%. This small change in P_u/P_0 does not warrant changing $k_2\,e_c'$ and $k_3\,e_{cu}$ and as previously indicated values of 0.002 and 0.0035 respectively were adopted when computing the data for all the included design charts.

Steels with yield stress f_{sy} varying from 30 to 60 ksi at ambient temperature can be used when designing chimneys. At 600° C $k_5\,e_{sy}$ can be 60% of its value at 20° C so that $k_5\,e_{sy}$ can vary from 0.0006 to 0.002. A 100% change in $k_5\,e_{sy}$ i.e., from 0.001 to 0.002 for the particular section shown on Fig. 8b causes a maximum variation of about 6% in the P_u/P_0 ratio. Although the author believes 6% variation in P_u/P_0 is negligible it was thought appropriate to include separate sets of graphs for the four different $k_5\,e_{sy}$ values of 0.0005, 0.001, 0.0015 and 0.002.

4.5. Effect of Temperature T

Change in temperature alters the strains $k_2\,e_c'$, $k_3\,e_{cu}$, $k_5\,e_{sy}$ and the stresses $k_1 f_c'$ and $k_4 f_{sy}$. It has been shown that changes in $k_2\,e_c'$, and $k_3\,e_{cu}$ have a negligible effect on P_u/P_0 and although variation of $k_5\,e_{sy}$ has little effect, charts for four different values have been prepared. The stresses $k_1 f_c'$ and $k_4 f_{sy}$ only occur in the steel ratio parameter q when computing e/r from Eqs. (26) or (35) and P_u/P_0 from Eqs. (28), (28a) or (36). Variation of $k_1 f_c'$ and $k_4 f_{sy}$ can therefore be accommodated by including a number of q constant curves. The ultimate strength design charts provided permit the designer to select these material stresses at will.

4.6. Design Example

A chimney section of base mean dia 40′ is subjected to a dead load ultimate axial force of 16,000 kips and a wind ultimate bending moment of 2,000,000 kip.in. The wall has a flue opening half angle $\beta=20°$ and is subjected to a mean temperature $T=100°$ C. Assuming that Portland cement gravel concrete

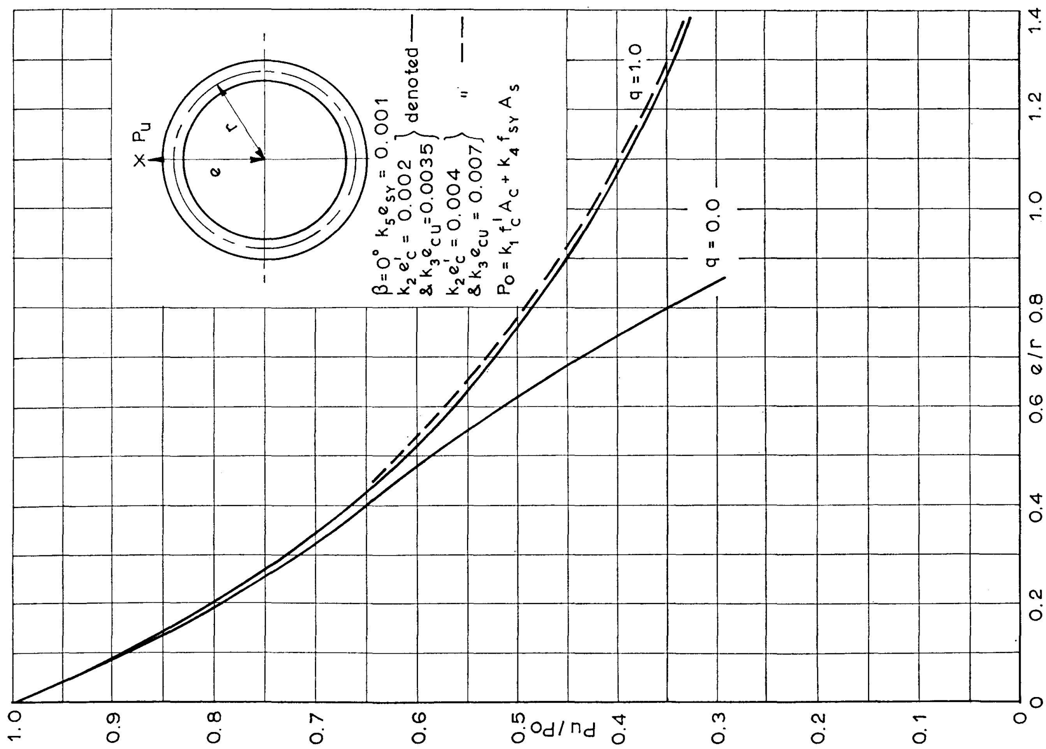

Fig. 8a. Comparison of variation of concrete strains $k_2 e_c'$ and $k_3 e_{cu}$.

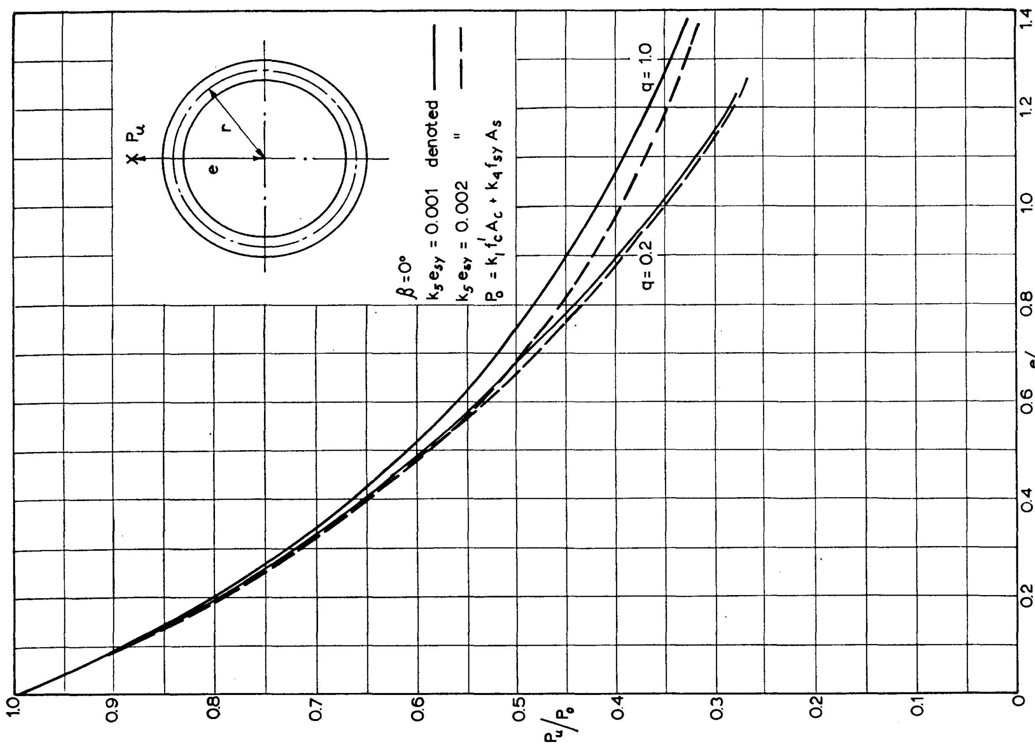

Fig. 8b. Comparison of steel strain $k_5 e_{sy}$ variation.

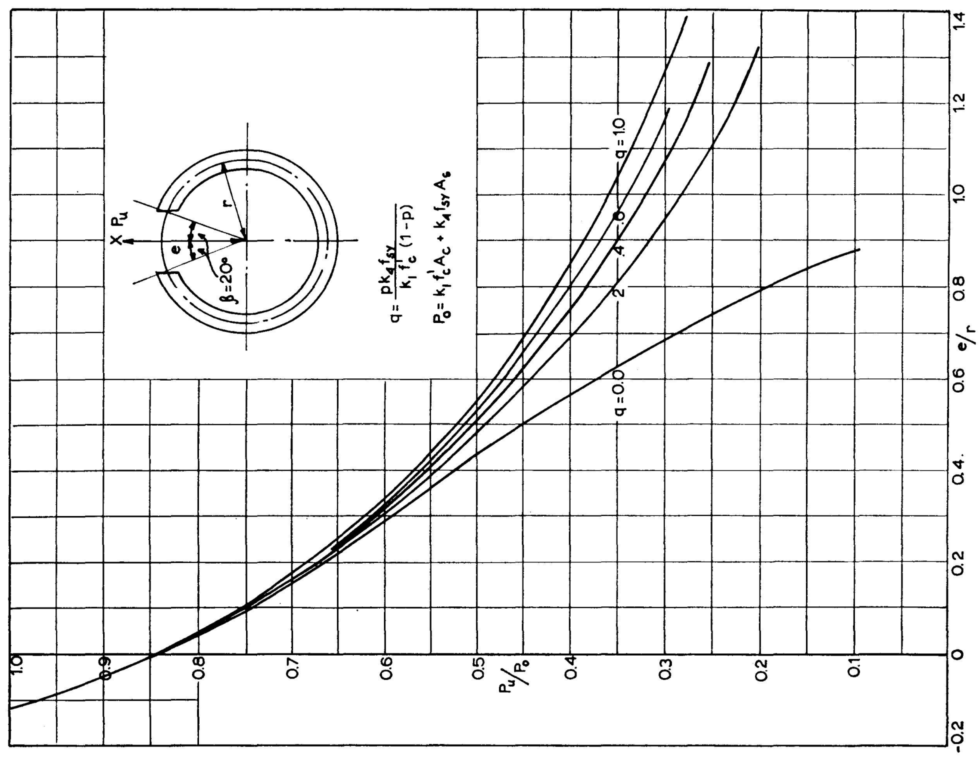

Fig. 9b. Ultimate strength design chart for $\beta = 20°$ and $k_5 e_{sy} = 0.0005$.

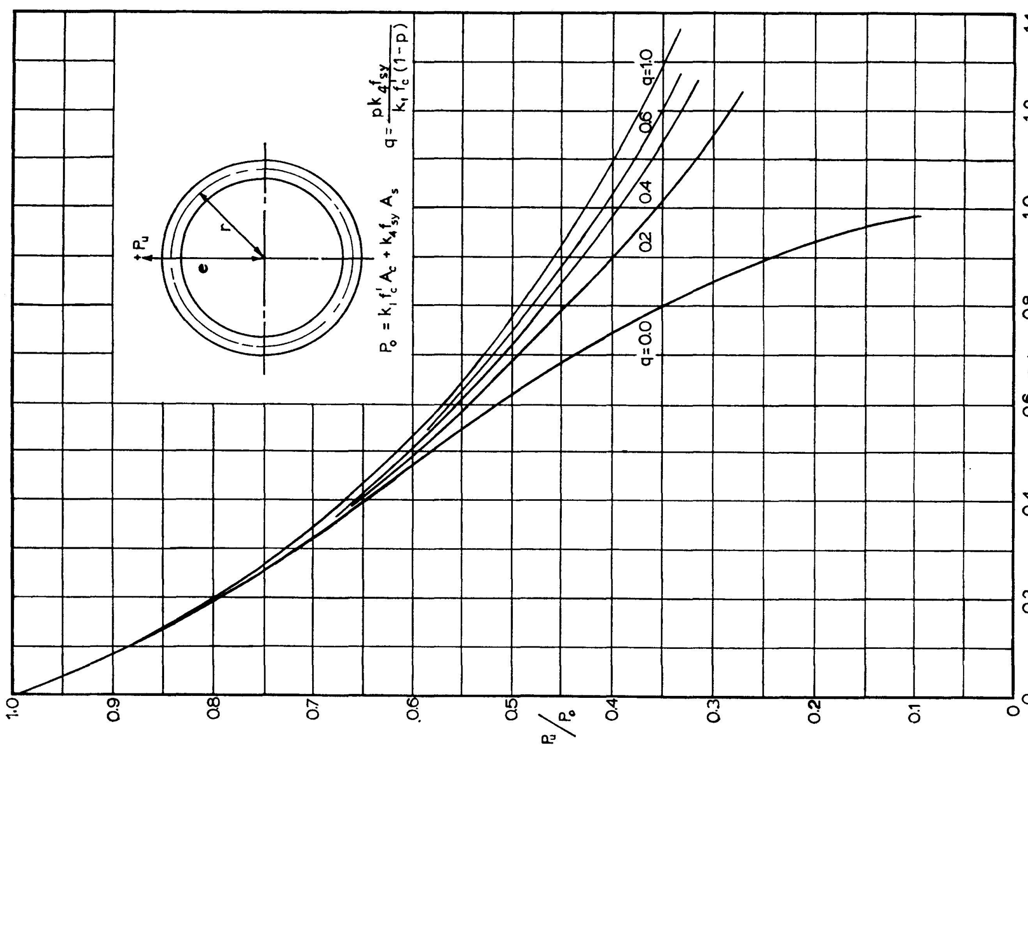

Fig. 9a. Ultimate strength design chart for $\beta = 0°$ and $k_5 e_{sy} = 0.0005$.

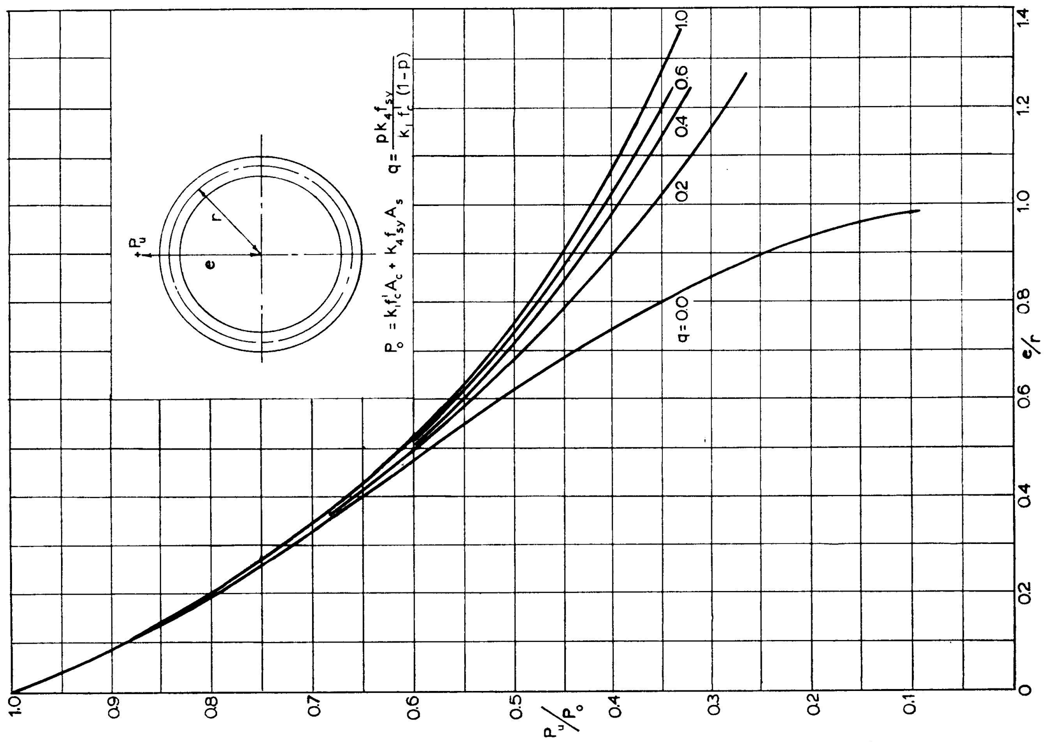

Fig. 10a. Ultimate strength design chart for $\beta = 0°$ and $k_5 e_{sy} = 0.001$.

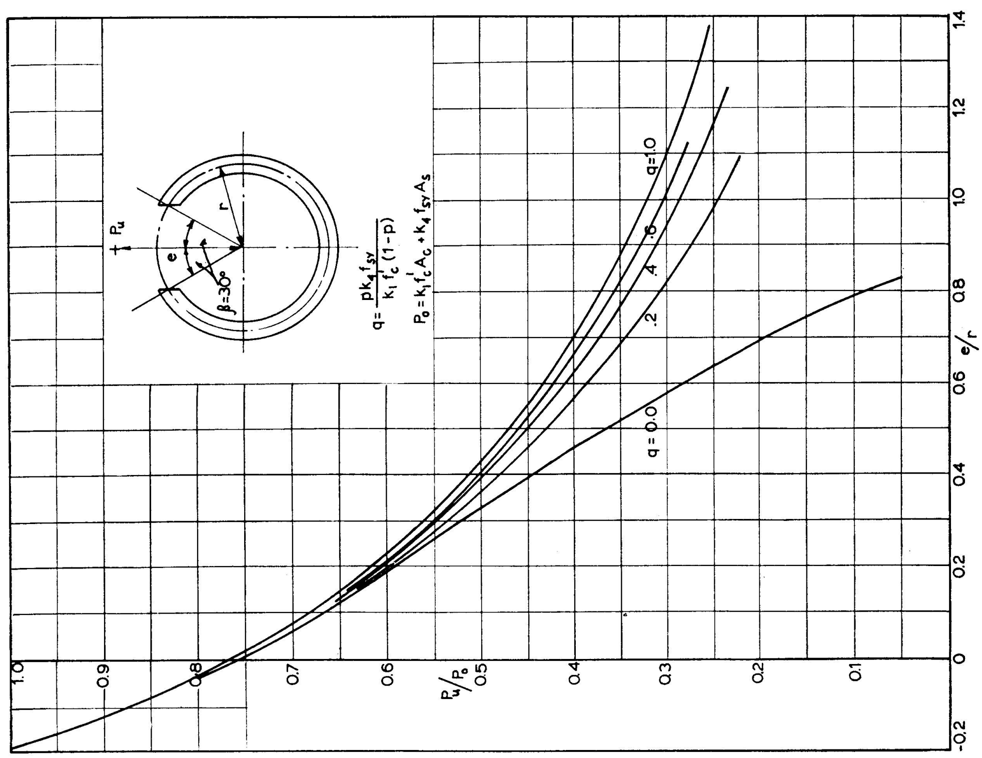

Fig. 9c. Ultimate strength design chart for $\beta = 30°$ and $k_5 e_{sy} = 0.0005$.

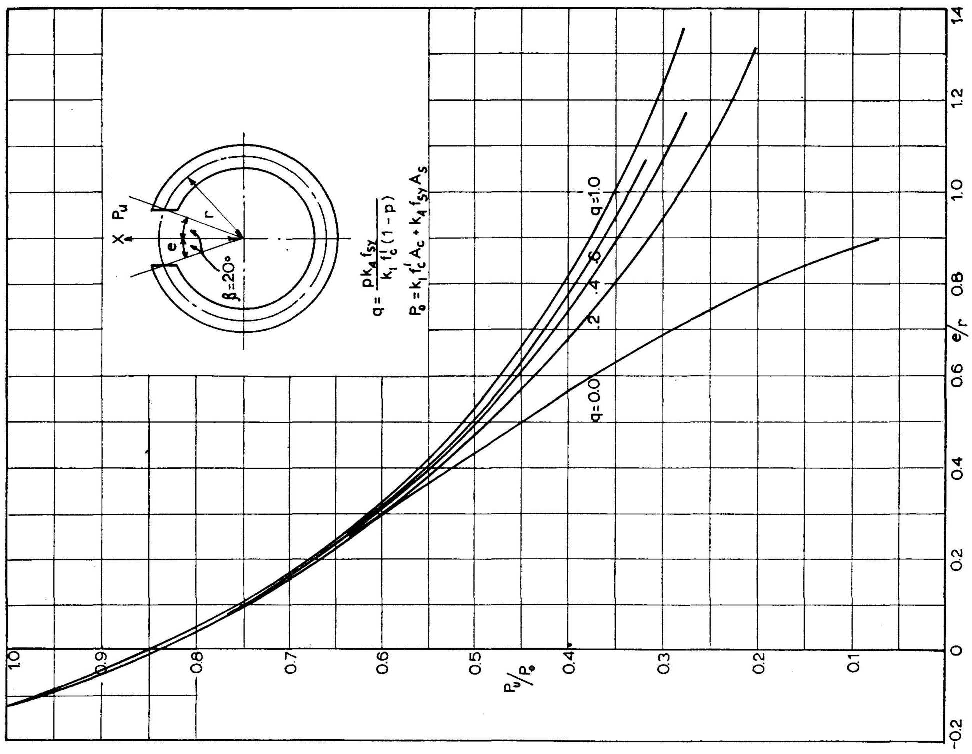

Fig. 10b. Ultimate strength design chart for $\beta = 20°$ and $k_5 e_{sy} = 0.001$.

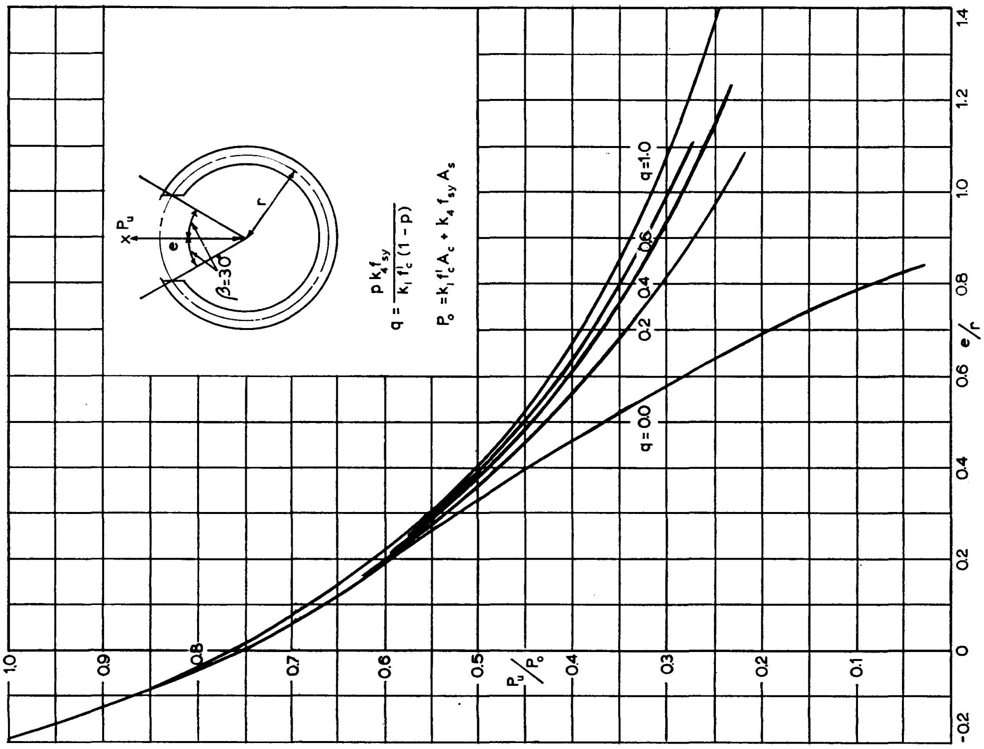

Fig. 10c. Ultimate strength design chart for $\beta = 30°$ and $k_5 e_{sy} = 0.001$.

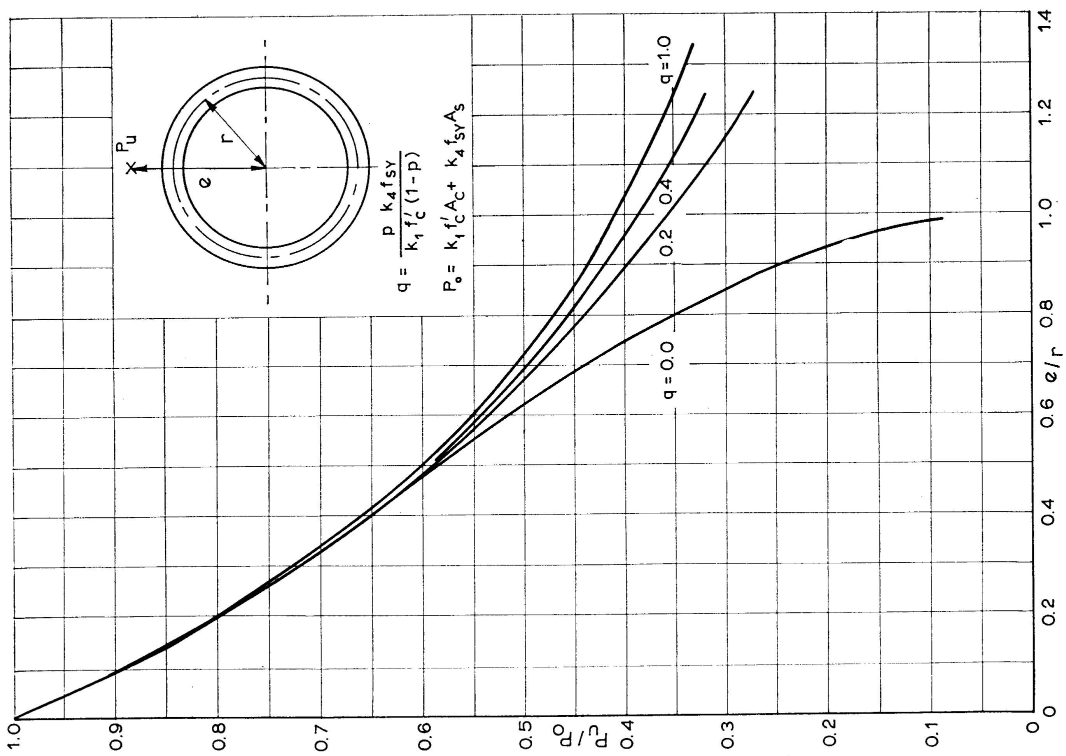

Fig. 11a. Ultimate strength design chart for $\beta = 0°$ and $k_5 e_{sy} = 0.0015$.

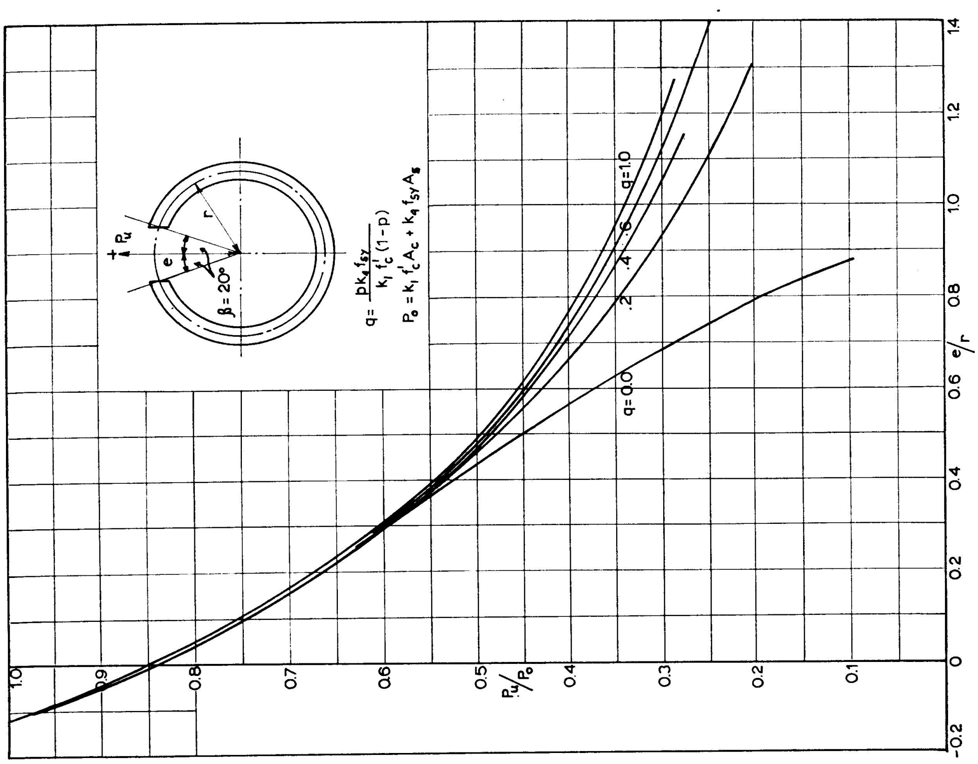

Fig. 11b. Ultimate strength design chart for $\beta = 20°$ and $k_5 e_{sy} = 0.0015$.

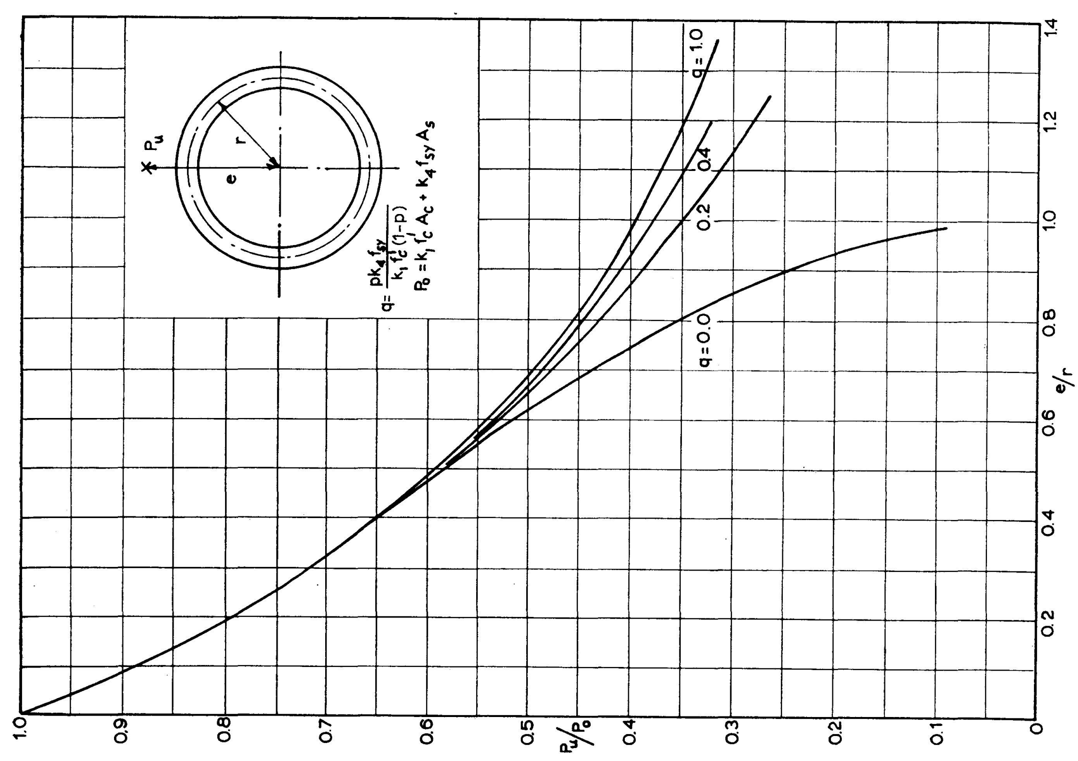

Fig. 12a. Ultimate strength design chart for $\beta = 0°$ and $k_5 e_{sy} = 0.002$.

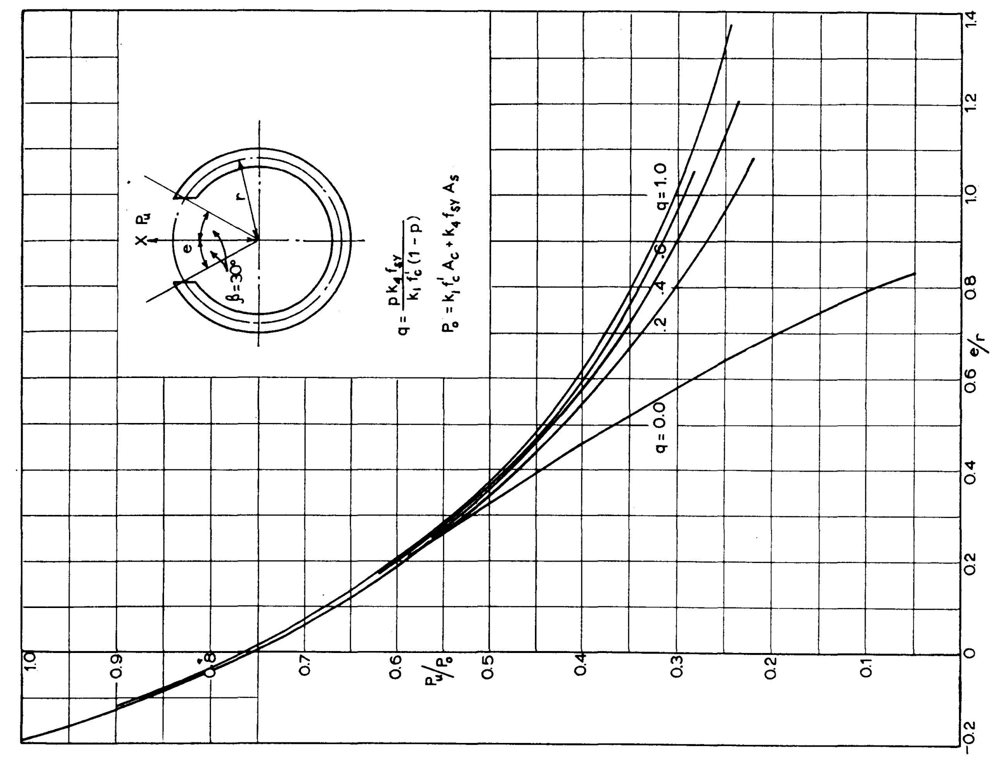

Fig. 11c. Ultimate strength design chart for $\beta = 30°$ and $k_5 e_{sy} = 0.0015$.

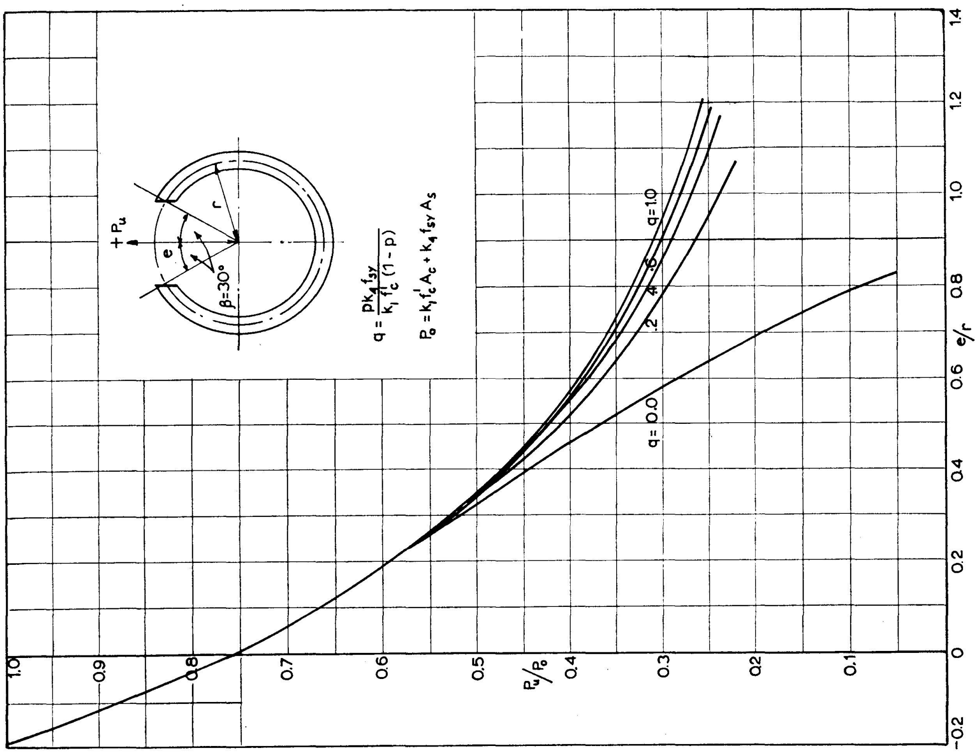

Fig. 12c. Ultimate strength design chart for $\beta = 30°$ and $k_5 e_{sy} = 0.002$.

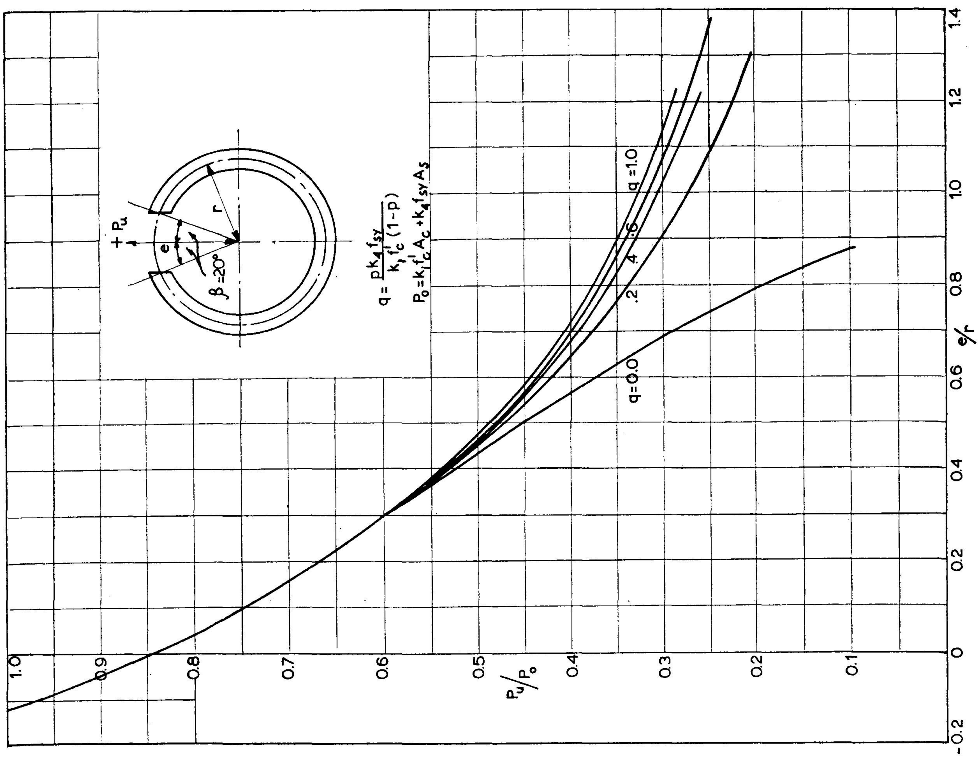

Fig. 12b. Ultimate strength design chart for $\beta = 20°$ and $k_5 e_{sy} = 0.002$.

of compressive strength $f_c' = 4\,\text{ksi}$ and structural grade steel of yield stress $f_{sy} = 33\,\text{ksi}$ are to be used, design a satisfactory cross-section at the chimney base.

From Figs. 2 and 3 $k_1 = 0.6$ Then $k_1 f_c' = 2.4\,\text{ksi}$,

$k_2 = 1.0$ $k_2 e_c' = 0.002$,

$k_4 = 0.95$ $k_4 f_{sy} = 31.4\,\text{ksi}$.

$k_5 = 0.95$ $k_5 e_{sy} = 0.00104 \cong 0.001$.

Assuming the wall thickness $t = 10''$ and the steel proportion $= 0.01$ then the wall mean radius $r = 240\,\text{in.}$, the effective concrete area $A_c = 2 \times 240 \times 10\,(\pi - 0.348)(1 - 0.01) = 13{,}250\,\text{in}^2$, the steel area $A_s = 2 \times 240 \times 10\,(\pi - 0.348)\,0.01 = 134\,\text{in}^2$.

$$\therefore\; P_0 = 2.4 \times 13{,}250 + 31.4 \times 134 = 36{,}000 \text{ kips}.$$

Now eccentricity $$e = \frac{2{,}000{,}000}{16{,}000} = 125 \text{ in.}$$

$$\frac{e}{r} = \frac{125}{240} = 0.52,$$

steel ratio $$q = \frac{31.4 \times 0.01}{2.4\,(1 - 0.01)} = 0.132.$$

From Fig. 10b $$\frac{P_u}{P_0} = 0.46,$$

$$\therefore\; P_u = 0.46 \times 36{,}000 = 16{,}600 \text{ kips} > 16{,}000,$$

$\therefore$ adopt a $10''$ wall thickness.

5. Concluding Remarks

1. A procedure for determining the effect of elevated temperature on the flexural strength characteristics of reinforced concrete materials is suggested.
2. Ultimate strength analysis of hollow circular reinforced concrete sections is proposed.
3. Ultimate strength design charts for three sizes of flue opening and four different grades of steel are included for the direct design of chimneys.
4. Large variation of the values of several important design parameters show small effect on the ultimate strength ratio P_u/P_0 thereby minimizing the required number of the design charts.
5. The observed results of seven thin wall circular concrete specimens without flue openings, tested at ambient temperature in the Structures Laboratory of the Civil Engineering School, agree with the theoretical strengths predicted by the proposed theory within about 10%. No static or dynamic load tests could be found in the literature.
6. No experimental evidence could be found on the effect of ovalization, crinkle buckling, slenderness ratio, wind vibration, acidic gas attack, or work-

manship on the ultimate strength of hollow concrete sections and these factors have not been considered in the proposed theory.

6. Acknowledgements

This paper forms part of a study of the ultimate strength of thin wall concrete members in biaxial bending being conducted in the School of Civil Engineering at the University of New South Wales. The computer programmes were run by the Electrical Engineering School staff on their IBM 360/50 computer. The author wishes to thank Professor A. S. Hall for his general encouragement and Mr. J. M. Taylor for his production of computer data and the resulting design charts.

Key Words

Structural engineering, reinforced concrete, ultimate strength, bending and compression, temperature effects, computer.

7. Notation

P_0 = load at failure when placed at the plastic centre of the cross-sectional area.

P_u = load at failure when placed at an eccentricity e measured from the centre of the circle forming the section shape.

r = mean radius of the hollow section.

d = mean diameter of the hollow section.

t = wall thickness of the hollow section.

L = effective length of chimney.

e = eccentricity of compressive force P_u measured from the centre of the circle forming the section shape.

A_c = effective concrete cross-sectional area $= 2(1-p)\, r\, t\, (\pi-\beta)$.

A_s = total steel area in cross-section.

p = proportion of steel reinforcement in section $= A_s/2\, r\, t\, (\pi-\beta)$.

f_c = concrete stress.

f_c' = maximum concrete compressive stress obtained in a control cylinder test at ambient temperature.

E_c = concrete modulus of elasticity at any temperature $= \dfrac{k_1 f_c'}{k_2 e_c'}$.

f_s = steel stress.

f_{sy} = steel yield stress at ambient temperature.

E_s = steel modulus of elasticity at any temperature $= \dfrac{k_4 f_{sy}}{k_5 e_{sy}}$.

q = reinforcement ratio $= \dfrac{k_4 f_{sy}\, p}{k_1 f_c' (1-p)}$.

e_c = concrete strain.

e_c' = concrete strain when maximum stress f_c' is first attained in a control cylinder at ambient temperature.

e_{cu} = maximum concrete compressive strain at failure in a hollow section with tension over portion of the cross-section and at ambient temperature.

e_1 = compressive strain in concrete extreme upper fibre shown by point 1 in Fig. 4.

e_{s1} = compressive strain in steel extreme upper fibre shown by point $s\,1$ in Fig. 4.

e_2 = strain in steel extreme lower fibre shown by point 2 in Fig. 4.

e_s = steel strain.

e_{sy} = steel yield strain at ambient temperature.

T = concrete chimney shell mean elevated temperature.

k_1 = ratio of concrete ultimate strength at temperature T to its ultimate strength f_c' at ambient temperature taken as 20° C.

k_2 = ratio of concrete strain at temperature T to its strain e_c' at ambient temperature, both strains occurring when maximum stress is first attained.

k_3 = ratio of maximum value of extreme fibre strain in flexure at temperature T to its maximum strain e_{cu} at ambient temperature.

k_4 = ratio of steel yield stress at temperature T to its yield stress f_{sy} at ambient temperature.

k_5 = ratio of steel yield strain at temperature T to its yield strain e_{sy} at ambient temperature.

Q = total compressive force in the steel.

R = total compressive force in the concrete.

S = total tensile force in the steel.

Q', R', S' = either the moment of Q, R or S respectively about the neutral axis when the neutral axis is within a section or the moment of Q, R or S respectively about the extreme lower steel fibre when the neutral axis is outside the section.

A_1, B_1, C_1, D_1 = non-dimensional trigonometric functions relevant only when the neutral axis is inside a section at failure.

A_2, B_2, C_2, D_2 = non-dimensional trigonometric functions relevant only when the neutral axis is outside a section at failure.

The following angles are all measured at the centre of the circle forming the section shape. They are measured from the centre line of the flue hole to some point on the mid-wall position.

α = angle defining a point on the mid-wall position through which the neutral axis passes.

β = angle defining a point on the mid-wall position that fixes the size of the flue opening.

θ = variable angle defining a typical point on the mid-wall position.
θ_3 = angle defining the point 3 shown in Fig. 4 at which the concrete strain equals $k_2 e_c'$.
θ_4 = angle defining the point 4 shown in Fig. 4 at which the steel compressive strain equals $k_5 e_{sy}$.
θ_5 = angle defining the point 5 shown in Fig. 4 at which the steel tensile strain equals $k_5 e_{sy}$.

8. References

1. American Concrete Institute Committee 505. "Specification for the Design and Construction of Reinforced Concrete Chimneys." ACI 505–54, Jour. A.C.I., Vol. 26, Sept. 1954, pp. 1–48 (Proc. A.C.I., Vol. 51).
2. Malhotra, H. L.: The Effect of Temperature on the Compressive Strength of Concrete. Mag. of Conc. Research, Vol. 28, No. 23, Aug. 1956, pp. 85–94.
3. Saemann, J. C. and Washa, G. W.: Variation of Mortar and Concrete Properties with Temperature. Jour. A.C.I., Vol. 29, No. 5, Nov. 1957, pp. 385–395.
4. Brettle, H. J.: The Flexural Strength and Elastic Properties of Pre-tensioned Concrete Beams of Rectangular Cross-Section. Ph.D. thesis, School of Civil Engg., Univ. of New South Wales, 1958, 399 p.
5. Zoldners, N. C.: Effect of High Temperatures on Concretes Incorporating Different Aggregates. Proc. A.S.T.M. Philadelphia, Vol. 60, 1960, pp. 1087–1108.
6. Taylor, C. P. and Turner, L.: Reinforced Concrete Chimneys. Concrete Pubs., Second Edit. 1960, 81 p.
7. American Concrete Institute and Cement and Concrete Association on "Recommendations for an International Code of Practice for Reinforced Concrete", A.C.I., 1965, 156 p.
8. Harmathy, T. Z. and Berndt, J. E.: Hydrated Portland Cement and Lightweight Concrete at Elevated Temperatures. Jour. A.C.I., No. 1, Jan. 1966, pp. 93–112 (Proc. A.C.I., Vol. 63).
9. Campbell-Allen, D. and Desai, P. M.: The Influence of Aggregate on Behaviour of Concrete at Elevated Temperatures. Nuclear Eng. and Design, Vol. 6, No. 1, Aug. 1967, pp. 65–77.
10. Copeland, W. R. and Woodman, G. C.: The Behaviour of Reinforcing Steels at Elevated Temperatures. Jour. I.E. Aust., Vol. 38, No. 3, March 1966, pp. 53–59.
11. Hannant, D. J.: Effects on Strength of Various Concretes of Sustained Temperatures near 100°C. Civil Engg. and Pub. Wks. Review, June 1967, pp. 665–667.
12. Brettle, H. J. and Warner, R. F.: Theory for the Ultimate Strength Design of Hollow Circular Reinforced Concrete Sections. Civil Engg. Trans. I.E. Aust., Vol. CE 9, No. 2, Oct. 1967, pp. 242–248.
13. Warner, R. F. and Brettle, H. J.: Ultimate Strength Design of Thin-Wall Circular Bridge Piers. Int. Assoc. for Bridge and Struct. Engg., Vol. 27, 1967, pp. 255–270.
14. Warner, R. F. and Brettle, H. J.: Strength of Reinforced Concrete in Biaxial Bending and Compression. Dept. of Civ. Engg., Univ. of New South Wales, Uniciv Report No. R-24, Nov. 1967, 29 p.
15. Stelle, W. W.: Tallest smoke stack for Mitchell Plant. Civil Engg., A.S.C.E., March 1969, pp. 44–47.
16. Leonhardt, F.: Modern Design of Television Towers. I.C.E. Lond., May 1969, pp. 265–291.

Summary

This paper describes the theoretical analysis of the ultimate strength of hollow circular reinforced concrete chimneys subjected to elevated temperatures. A method of design is suggested and design charts for three sizes of flue openings and four different grades of steel are included to simplify the design procedure.

No published results of ultimate strength tests of thin wall circular sections subjected to elevated temperatures can be found in the literature to compare with the proposed theory. Some observations of concrete test cylinders exposed to different heating and cooling procedures are available. Simplified approximations of the effect of elevated temperature on the ultimate strength characteristics of reinforced concrete materials are included to assist the design procedure.

Résumé

Le travail décrit l'analyse théorique de la charge de cheminées circulaires en béton armé exposées à de hautes températures. Une méthode de construction est proposée et des dessins pour trois différentes grandeurs d'ouverture de gaz d'échappement et pour quatre différentes qualités d'acier sont joints pour faciliter la procédure de construction.

Dans la littérature, on ne trouve pas de résultats de charges de sections circulaires à paroi mince sous l'influence de hautes températures, qui seraient comparables avec la théorie proposée. Il existe quelques observations d'éprouvettes cylindriques en béton, exposées à de différents modes de chauffage et de refroidissement. Des approximations simplifiées concernant des matériaux en béton sont également présentées dans ce travail.

Zusammenfassung

Die Arbeit beschreibt die theoretische Analyse der Traglast von kreisrunden Stahlbetonschornsteinen, die hohen Temperaturen ausgesetzt sind. Es wird eine Konstruktionsmethode vorgeschlagen und Zeichnungen für drei Grössen von Abgasöffnungen und vier verschiedene Klassen von Stählen gegeben, um das Konstruktionsvorgehen zu vereinfachen.

In der Literatur finden sich keine Resultate über Traglasten von dünnwandigen kreisrunden Querschnitten unter dem Einfluss hoher Temperaturen, die mit der vorgeschlagenen Theorie vergleichbar wären. Es bestehen einige Beobachtungen an Beton-Versuchszylindern, die verschiedenen Heiz- und Kühlvorgängen ausgesetzt sind. Vereinfachte Näherungen über den Einfluss hoher Temperaturen auf die Traglast-Charakteristiken von Betonmaterial sind in der vorliegenden Arbeit inbegriffen.